KO-22/23: A Next Generation Supersonic Transport

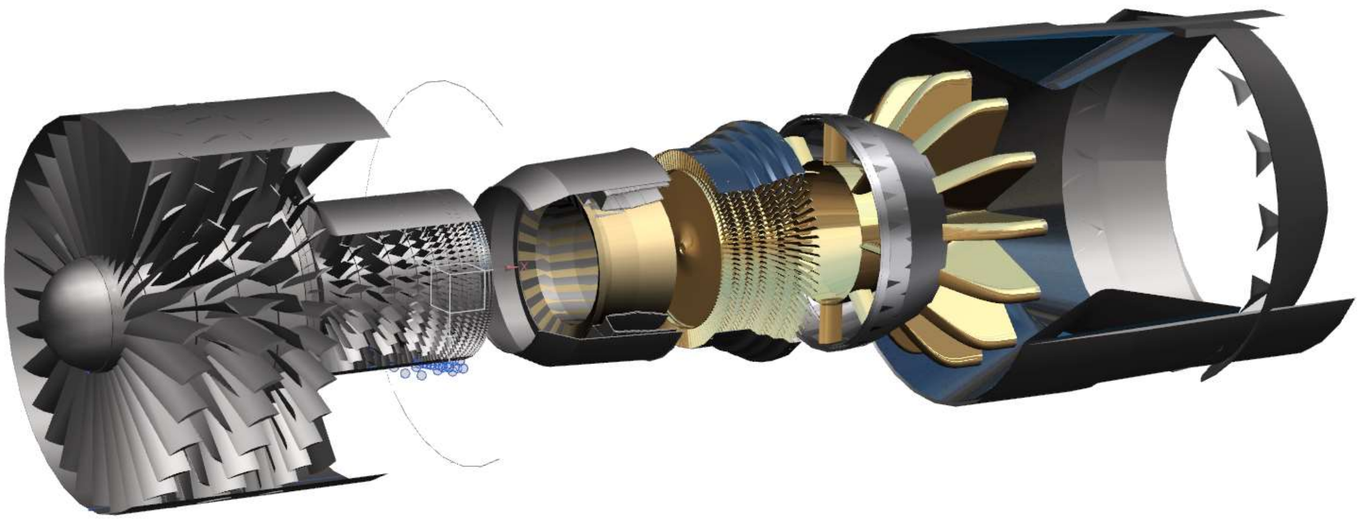

Department of Aerospace Engineering

Team: Total Incredible Technical Solution

KO-22/23: A Next Generation Supersonic Transport

Design Team:

Damian Maciorowski Damian Maciorowski

#919069

Karol Kozdrowicz Karol Kozdrowicz

#907241

Maciej Spychała Maciej Spychała

#921050

Karolina Pazura Karolina Pazura

#919607

Faculty Advisor:

Dr hab. Inż. Ryszard Chachurski ________________

#920758

Abstract

This report present a two-spool, mixed stream turbofan engine- KO-22/23. The main goals which were achieved:

- utilize the most modern technical solutions to bridge the gap between present and future
- lower Thrust Specified Fuel Consumption and Net Thrust
- reduced noise and pollution emissions were achieved due to application of modern solution in the combustion chamber and new, unique chevron concept
- minimize mass while maximizing efficiency and reliability for most conditions
- used bladed rings (bling) technology simultaneously with variable trailing edges of fan blades
- higher turbine inlet temperature

Due to the fact that engine KO-22/23 would be implemented in airliners the main assumption was to improve aspects like cost, simplification of service and lifetime of propulsion. Modern materials to increase temperature at combustion exit, which decrease TSFC and increase thrust and to simultaneously reduced weight.

Tabel of Contents:

List of Tables:

List of figures:

List of equations:

List od Symbols

Latin	Definition	Unit
A	Area	ft^2
A_0	Inlet air demand passing through the inlet throat area	ft^2
A_c	Capture area	ft^2
A_{byp}	Inlet engine bypass air area	ft^2
A_{0eng}	Engine demand flow area	ft^2
A_{OI}	Inlet air demand in the freestream area	ft^2
A_{ref}	Combustor reference area	ft^2
A_{0spl}	Inlet spillage area	ft^2
C	Absolut velocity	ft/s
C_p	Heat constant	ft/s
C_d	Drag factor of inlet	-
C_u	Absolute Swirl FLow Velocity	ft/s
C_x	Axial velocity	ft/s
b	Combustor reaction rate parameter	-
e	Euler's constant	-
h	Combustor height	in
h	Enthalpy	
D	Drag of inlet, diameter	lbf
eRam	Inlet recovery(selected on the basis of charts from RFP)	-

k	Isentropic coefficient	-
l	Length dimension, work	in
L_d	Length of diffusor	in
$\dot{m}_t$	Combustor inlet mass flow	lb/s
$\dot{m}$	Mass flow	lb/s
p	Pressure	psi
P_f	Profile factor	-
P_3	High pressure compressor exit static pressure	psi
P_{t4}	Combustor exit total pressure	psi
Q	Divide coefficient	-
R	Gas constant, radious	BTU/lbm-◦R,in
R	Current radius	in
R	Tip radius of shield	in
R_o	Radius of hole	in
R_m	Pitch radius	in
R_t	Tip radius	in
R_h	Hub radius	in
N	Rotational speed	1/min
T	Temperature	^0R
T_4	Combustor exit total temperature	^0R
U	Peripheral speed	ft/s
W	Relative velocity, velocity of fluid in relative frame of reference	ft/s

Greek	**Definition**	
α	Turbine absolute angle	deg
α	Compressor absolute angle	deg
β	Compressor relative angle	deg
β	Plane oblique shock wave angle	deg
β	Turbine relative angle	deg

β	Thermal expansion coefficiency	deg
ϵ	Modulus of longitudinal elasticity	psi
σc	Total stress	psi
σ_r	Radial tension	psi
σ_u	Perpheral tension	psi
ϑ	Poisson coefficient	-
$2\phi_D$	Diffuser angle of convergence	deg
δ_n	Nozzle speed coefficient	-
δ	Rotor speed coefficient	-
π_s*	Total pressure ratio	-
ρ	Density	lb/in3
η_s*	Coefficiency of compressor	-
μ	Load coefficient	-
ρ	Degree of reaction on pitchline	-
τ_1	First ramp angle	deg
Y_0	Dimension between the fan axis and the middle of the throat area in	
ω_{HPT}	Rotating speed	1/min

Subscipts

1,2,3,4..	Sections up
bld	Bleed
byp	Bypass
cowl	Cowl lip section
des	Design
diff	Diffusor
ell	Elliptic curvature
EX	End of external compression in inlet
NS	Normal direction shock
local	Stream before inlet
req	Rectangular part
T	Total
Th	Throat of inlet

spill	Inlet spillage
Wid	Width dimension

Abbreviations and acronyms

ACE	Adaptive Cycle Design
BPR	Bypass Ratio
CLP	Lefebvre Combustor Loading Parameter
CMC	Ceramic matrix composites
ECF	Emission Control Fuel Nozzle
EPA	Environmental Protection Agency
EPNdB	Effective perceived noise in decibels
FN	Net Thrust
FPR	Fan Pressure Ratio
HPC	High Pressure Compressor
LPC	Low Pressure Compressor
HPT	High Pressure Turbine
LPT	Low Pressure Turbine
IGV	Inlet Guide Vanes
JAXA	Japan Aerospace Exploration Agency
LSF	Lean Staged Fuel Nozzle
MTOW	Maximal take-off weight
NPR	Nozzle pressure ratio
OPR	Overall Pressure Ratio
PF	Pattern factor
PR	Pressure Ratio
RFP	Request For Proposal
RPM	Rounds per minute
SLS	Sea Level Standard
s NOX	NOx emission index
TPR	Total pressure recovery
TRL	Technology readiness levels
TSFC	Thrust Specified Fuel Consumption
WF	Burner-Fuel Mass Flow

1. Introduction

In this report our team wanted to present a unique candidate engine to drive next generation supersonic aircraft. KO-22/23 is 2-spool, average bypass ratio turbofan that includes all of the most modern technologies and unique technical solutions to provide the safest, fastest and possibly most affordable transport by over 3400 nmi. Basic engine view with his destination is shown in Figures 1.1 and 1.2 followed by aircraft characteristic in Table 1.1[1.1].

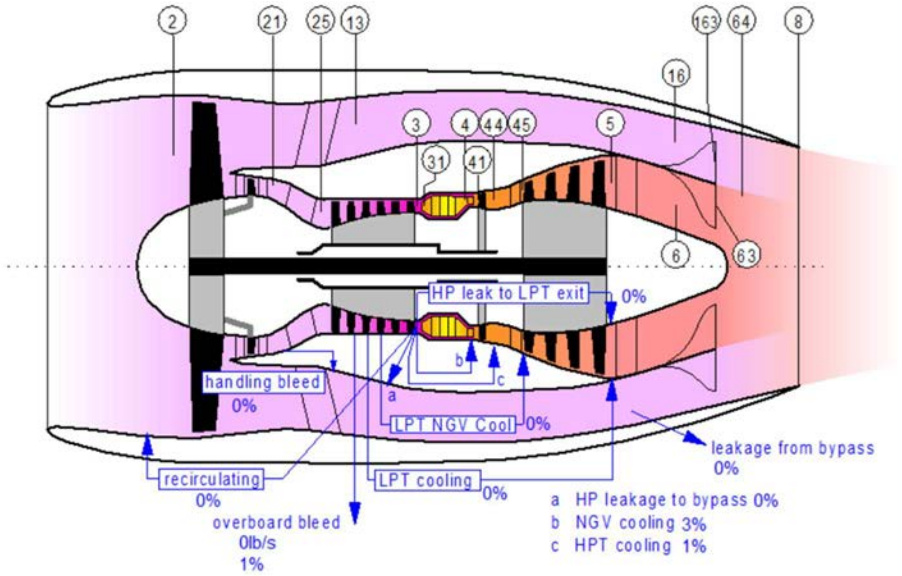

Figure 1.1. Schematic KO-22/23 flowpath cross-section

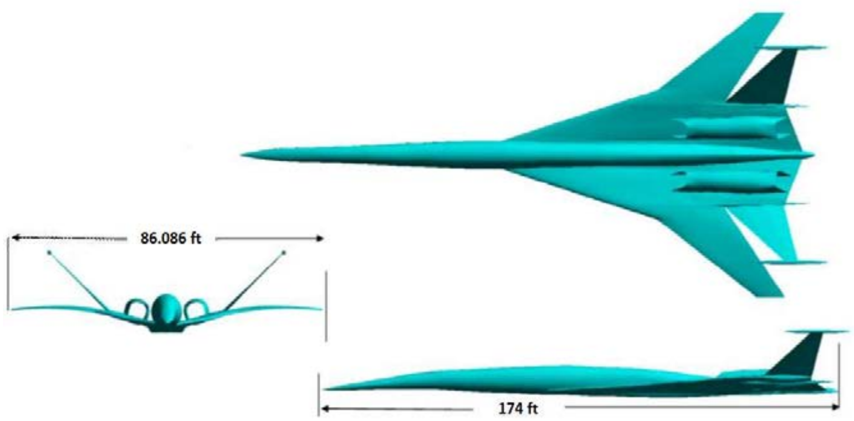

Figure 1.2. NASA aircraft concept (765-076F configuration)[1.2]

General characteristics	
Max. take-off weight	317,499 lb
Payload weight	21,000 lb
Operating empty weight	146,420 lb
Wing loading (takeoff)	77.5 psf
Power plant	2 × mixed-flow turbofans; 61,000 lbf each @ SLS
Performance	
Maximum speed	Mach 1.8 at 55,000 feet
Cruise speed	Mach 1.6 at 50,000-55,000 feet
Range	4000 nmi
Cruise L/D	9.2

Table 1.1. Aircraft general characteristics

Candidate engine was obliged to exceed by 5% Net Thrust and Thrust Specified Fuel Consumption (TSFC) that are shown in Table 1.2.

	Net Thrust (lbf)	TSFC (lbm/hr/lbf)
SLS	64625	0.520
Hot Day Take-Off	56570	0.652
Transonic Pinch	14278	0.950
Supersonic Cruise	14685	1.091

Table 1.2. Net Thrust and TSFC requirements.

All the following considerations includes cycle design and optimization to make KO-22/23 a serious contender, as well at design as off-design conditions. As the competition run on civil supersonic transport, this report focuses on minimizing cruise TSFC. Nevertheless a lot attention was paid to meet Take-Off requirements along with environmental friendliness.

2. Cycle analysis

2.1 Adaptive Cycle Engine (ACE) Design Concept

At the very first stage of this designing process ACE concept was taken into consideration. This idea gives a chance to optimize the engine for every step of a mission. However, this idea was blind alley because it is more complicated to apply some of necessary technical solutions, therefore more expensive avionics have to be used, thus raising the overall price and mass of the engine.

Furthermore ACE is a very popular concept mostly for a military aviation right now.

Civil transport law is much stricter than military’s so that’s leads to a conclusions that ACE concept would not be ready to implement in 2025.

2.2 Mixed-flow turbofan with average bypass ratio

After the rejection of the ACE concept, KO-22/23 started being perceived as a 2-spool mixed-flow turbofan with bypass ratio (BPR) between 1.9 and 3. Such a concept includes a multi-stage compressor with high summary pressure ratio. This leads to very satisfying cycles without needs to apply higher total temperatures at the exit of the combustor chamber than 3200 °R. Furthermore, due to having a simpler structure KO-22/23 will be cheaper and lighter compering to previous idea which is another substantiation for this concept .

2.3 Engine main components

KO-22/23 consist of nine main component:

1. Supersonic inlet
2. 2-stage Fan module preceded by Inlet Guide Vanes (IGV)
3. 1-stage Booster
4. 11-stage Axial High Pressure Compressor
5. Combustor chamber
6. 2-stage High Pressure Turbine
7. 4-stage Low Pressure Turbine
8. Mixer
9. Nozzle

	Fan Inlet	HPC Inlet	Combusor Inlet	HPT Inlet	LPT Inlet	Mixer	Nozzle Exit
Mass Flow [lb/s]	602,1	168,8	167,1	164,6	171,4	605,2	605,2
Total Temperature	589,8	760,4	1666,1	3194,0	2390,8	1105,9	1105,9
Static Temperature	556,8	724,8	1624,0	3189,5	2335,9	1093,3	757,4
Total Pressure [psia]	6,1	13,6	181,4	176,8	44,6	12,3	12,3
Static Pressure [psia]	35521,0	16377,0	164,0	175,7	40,4	11,8	3,1
Fuel-Air-Ratio [-]	0,000	0,000	0,000	0,027	0,026	0,007	0,007
Absolute Velocity [ft/s]	635,8	658,7	754,9	263,9	901,7	401,0	2084,6

Table 2.1 Flow parameters through the section

2.4 Engine Cycle Modelling Process

2.4.1 Selecting Base Engine Cycle

The first step to model an engine that could meet supersonic cruise requirements. This was achieved using GasTurb 13 software. Requirements attached to the RFP were given in section 1 in Table1.2. The most important step of a supersonic transport mission is the supersonic cruise. A cycle was thus selected and optimized to cruise speed and altitude (1.6 Mach at 52500 ft.).

Results of this venture is shown in Figure 2.2 that presents Cycle Design of engine here and after the cycle, called Base Engine.

```
            W          T          P        WRstd
Station   lb/s         R        psia       lb/s      FN        =  15948,30 lb
 amb                389,97     1,492
  1     618,192     589,81     6,343                 TSFC      =    0,9891 lb/(lb*h)
  2     618,192     589,81     6,105   1587,000      WF Burner=   4,38195 lb/s
 13     405,755     763,69    13,894    520,769      s NOX     =    1,9319
 21     212,437     763,69    13,894    272,654      BPR       =    1,9100
 25     212,437     763,69    13,755    275,408      Core Eff  =    0,6136
  3     191,193    1767,11   224,739     23,077      Prop Eff  =    0,7913
 31     165,489    1767,11   224,739                 P3/P2     =    36,815
  4     169,871    3273,60   217,997     28,769
 40     176,031    3225,16   217,997                 NGV        2 Stage HPT
 41     188,353    3136,93   217,997     31,226      P16/P6    =   1,02449
 43     188,353    2208,44    38,804                 A63       =   3551,05 in²
 44     194,513    2195,29    38,804                 A163      =   3367,30 in²
 45     210,977    2135,92    38,028    165,454      A64       =   6918,35 in²
 49     210,977    1703,28    13,423                 XM63      =   0,22084
  5     215,757    1696,47    13,423    427,191      XM163     =   0,28577
  6     215,757    1696,47    13,155                 XM64      =   0,25990
 16     405,755     763,69    13,477                 P63/P6    =   0,99000
 64     621,512    1105,74    13,156                 P163/P16  =   0,99000
  8     621,512    1105,74    12,964   1028,692      A8        =   3174,31 in²
Bleed     1,062    1767,11   224,740                 CD8       =   0,95000
-------------------------------------------------    Ang8      =     25,00 °
Efficiencies:     isentr  polytr    RNI      P/P     P8/Pamb   =   8,69140
 Outer LPC        0,8923  0,9039  0,357   2,276      WLkBy/W25=    0,00000
 Inner LPC        0,8923  0,9039  0,357   2,276      WCHN/W25  =   0,08700
 HP Compressor    0,8534  0,8958  0,590  16,339      WCHR/W25  =   0,02900
 Burner           0,9995                  0,970      Loading   =    100,00 %
 HP Turbine       0,9098  0,8916  1,815   5,618      WCLN/W25  =   0,07750
 LP Turbine       0,9122  0,9013  0,492   2,833      WCLR/W25  =   0,02250
 Mixer            0,5000                             WBHD/W21  =   0,00000
-------------------------------------------------    far7      =   0,00710
HP Spool mech Eff 1,0000  Nom Spd    9850 rpm        WBLD/W25  =   0,00500
LP Spool mech Eff 1,0000  Nom Spd    4230 rpm        PWX       =     100,0 hp
-------------------------------------------------    P16/P13   =    0,9700
P2/P1= 0,9624 P25/P21=0,9900 P45/P44= 0,9800         P6/P5     =    0,9800
Con-Di Nozzle:                                       A9/A8     =   1,65800
 A9*(Ps9-Pamb)     1193,133                          CFGid     =   0,95159
```

Figure 2.2 Base engine cycle design

Base Engine perfectly meets requirements of cruise speed conditions, unfortunately its performance on Take-Off was insufficient. That is why more statistical data and trade studies were needed.

2.4.2 Parametric Studies And Cycle Selection

Parametric options are one of the many things that Gasturb 13 tools allow to obtain data and draw diagrams useful during parameters selection. This tool was used to make the following charts.

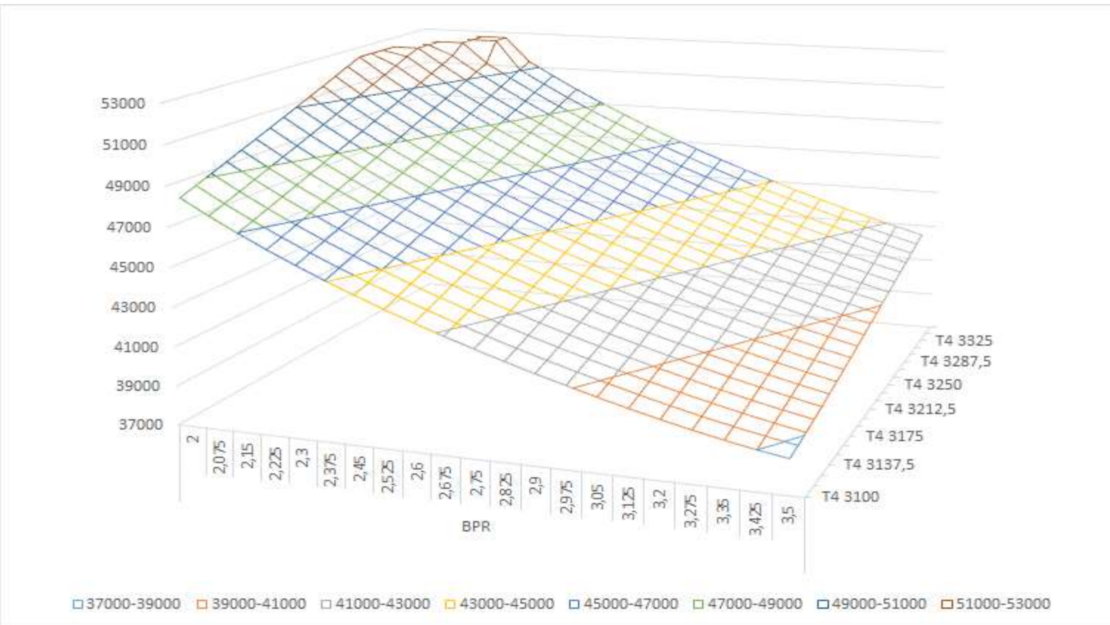

Figure 2.3 Chart showing Mission Fuel Burn*, Bypass Ratio and Turbine Inlet Temperature [°R]

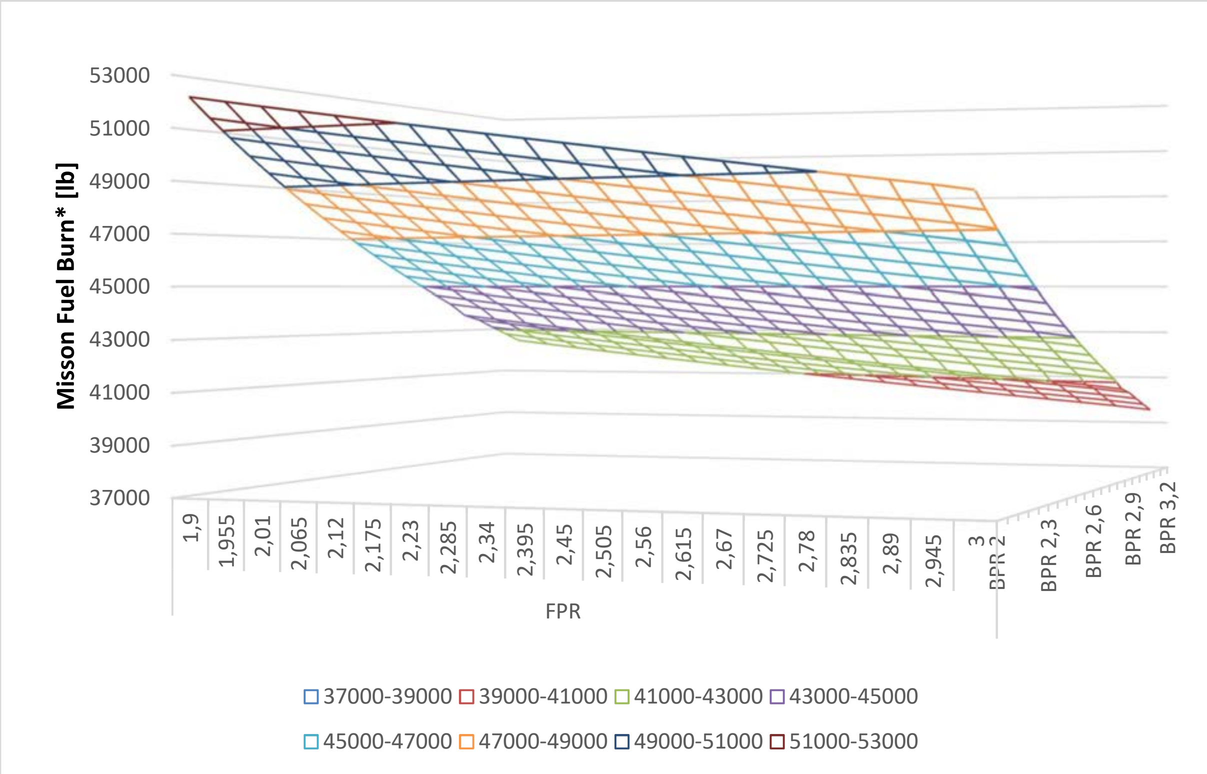

Figure 2.4. Chart showing Mission Fuel Burn*, Bypass Ratio and Fan Pressure Ratio

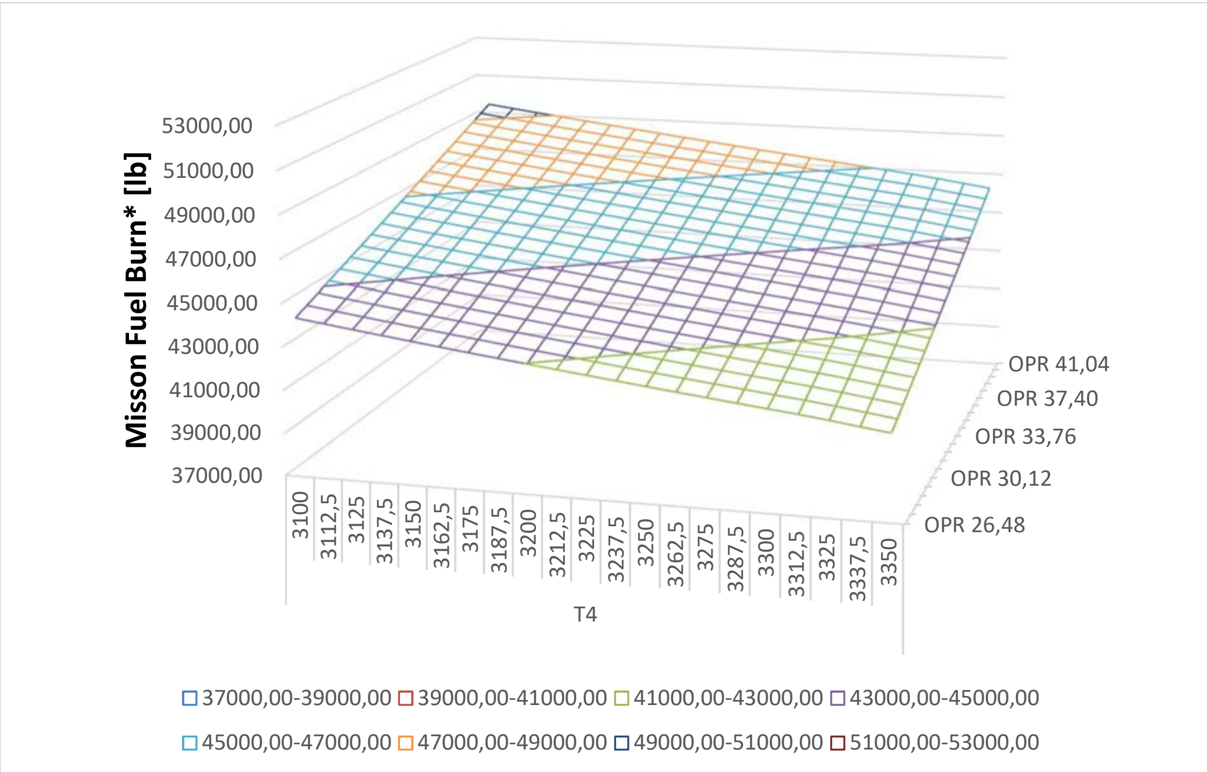

Figure 2.5 Chart showing Mission Fuel Burn*, Overall Pressure Ratio and Turbine Inlet Temperature [°R]

Figures 2.2-2.4 shows that lowering OPR and T4 whilst simultaneously increasing BPR will lead Base Engine to the most economical cycle. Nevertheless it stands to oppose another goal which is the assertion of Take-off Thrust. It is a very serious problem, due to the fact that we cannot fly into the air lowering TSFC. Thus, Figure 2.5 and 2.6 delivers some data of thrust increment trends.

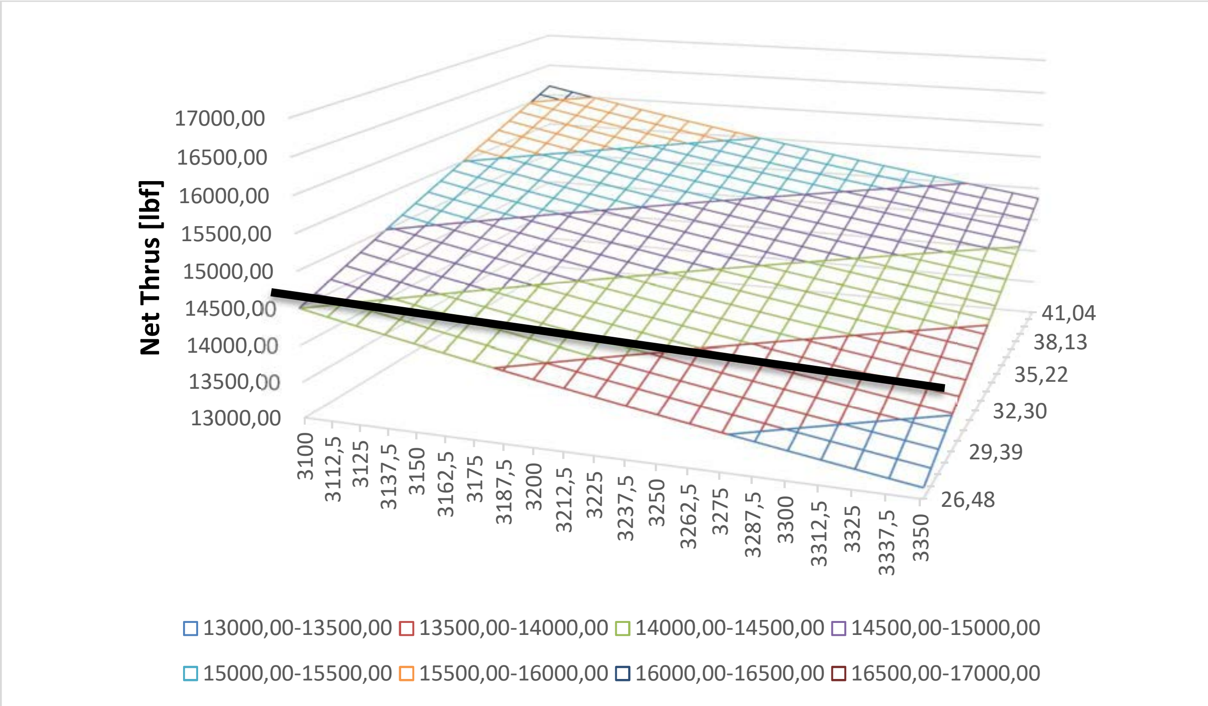

Figure 2.6. Chart showing Net Thrust, Turbine Inlet Temperature [°R] and Overall Pressure Ratio

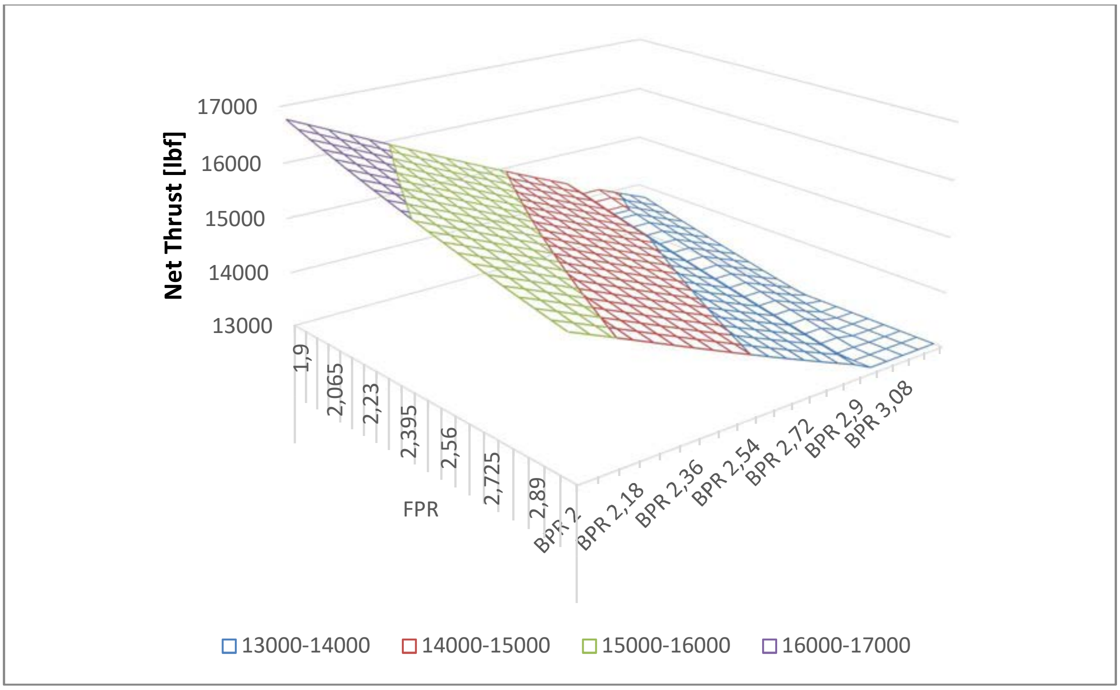

Figure 2.7. Chart showing Net Thrust, Fan Pressure Ratio and Bypass Ratio

Figures 2.5 shows that minimalizing OPR is no longer a key to optimize Basic Engine, all cycles below black line do not provide enough Thrust. At the same time it shows that at least 33 OPR is needed. If losses would be excluded and FPR would be tied 1.9 (from Figure 2.6) and 33 OPR together as the minimal values, High Pressure Compressor would have PR equal around 17.4.

The value of minimal OPR will change simultaneously with T4 and BPR changes but it still gives some data for correctly selected HPC PR.

Consideration about engine mass are more complicated. Since the lower OPR is chosen, the less number of stages is needed and reduce the engine weight. But when the higher OPR is selected that number of stages would increase which results in higher air density and lower radius dimensions which also affects positively on engine weight.

Eventually after selecting the parameters above and using trade studies to optimize between FPR, HPC PR, BPR and T4 values to get lowest TSFC while providing the required Thrust at the specified mission point, our team managed to set perfect parameters.

2.5 KO-22/23 Cycle presentation

The engine meets all the requirements that were set for it. KO-22/23 is light, economical, powerful and most importantly, it does not include any risky solution to boost its performance. As mentioned before, safety first.

```
            W          T          P        WRstd
Station   lb/s         R        psia        lb/s
 amb                389,97      1,492
  1     602,611     589,81      6,343
  2     602,611     589,81      6,105   1547,000
 13     433,789     735,57     12,193    622,614
 21     168,822     760,37     13,699    219,289
 25     168,822     760,37     13,562    221,504
  3     167,134    1666,12    181,357     24,274
 31     160,381    1666,12    181,357
  4     164,648    3194,00    176,805     33,961
 40     166,336    3179,79    176,805
 41     169,713    3152,16    176,805     34,775
 43     169,713    2397,06     45,522
 44     171,401    2390,37     45,522
 45     171,401    2390,37     44,611    121,214
 49     171,401    1947,76     16,943
  5     171,401    1947,76     16,943    288,094
  6     171,401    1947,76     16,604
 16     433,789     735,57     11,584
 64     605,190    1105,87     12,257
  8     605,190    1105,87     12,257   1059,521
Bleed     1,688    1234,56     63,557
-------------------------------------------------
Efficiencies:     isentr  polytr    RNI     P/P
 Outer LPC        0,8800  0,8910  0,357   1,997
 Inner LPC        0,8923  0,9037  0,357   2,244
 HP Compressor    0,8534  0,8936  0,585  13,373
 Burner           0,9970                  0,975
 HP Turbine       0,9077  0,8936  1,463   3,884
 LP Turbine       0,9122  0,9024  0,508   2,633
 Mixer            0,9854
-------------------------------------------------
HP Spool mech Eff 1,0000  Nom Spd    7800 rpm
LP Spool mech Eff 1,0000  Nom Spd    3476 rpm
-------------------------------------------------
P2/P1= 0,9624 P25/P21=0,9900 P45/P44= 0,9800
Con-Di Nozzle:
 A9*(Ps9-Pamb)     6096.940
```

```
FN         =  14829,43 lb

TSFC       =    1,0360 lb/(lb*h)
WF Burner=     4,26759 lb/s
s NOX      =    1,3286
BPR        =    2,5695
Core Eff =      0,6336
Prop Eff =      0,7986
P3/P2      =    29,708

NGV        2 Stage HPT
P16/P6     =   0,69763
A63        =    927,43 in²
A163       =   6568,13 in²
A64        =   7495,56 in²
XM63       =   0,77723
XM163      =   0,17340
XM64       =   0,25000
P63/P6     =   0,99000
P163/P16 =     0,99000
A8         =   3283,79 in²
CD8        =   0,94585
Ang8       =     27,07 °
P8/Pamb    =   8,21739
WLkBy/W25=     0,00000
WCHN/W25 =     0,03000
WCHR/W25 =     0,01000
Loading    =    100,00 %
WCLN/W25 =     0,00000
WCLR/W25 =     0,00000
WBHD/W21 =     0,00000
far7       =   0,00710
WBLD/W25 =     0,01000
PWX        =     100,0 hp
P16/P13    =    0,9500
P6/P5      =    0,9800
A9/A8      =   1,73159
CFGid      =   0.94628
```

Figure 2.8. KO-22/23 Supersonic Cruise Cycle Design

Figure 2.7 shows engine Supersonic Cruise Cycle Design. It provides 5% lower TSFC and higher Thrust compared to what was given in requirements. The engine parameters that lead to this are shown in table 2.1.

Summary Data			
Design MN	1.6		
Design Altitude	52500 ft		
Design Fan Mass Flow	602.611 lb/s		
Design Gross Thrust	43971.4 lbf		
Design Bypass Ratio	2.57		
Design Net Thrust	14809.85 lbf		
Design TSFC	1.0360		
Design Overall Pressure Ratio	29.9488		
Design Fan/LPC Pressure Ratio	Fan		LPC
	2		1.12
Design Chargeable Cooling Flow (%@25)	4		
Design Non-Chargeable Cooling Flow (%@25)	1		
Design Adiabatic Efficiency for Each Turbine	HPT		LPT
	0.9077		0.9122
Design Polytropic Efficiency for Each Compressor	Fan	LPC	HPC
	0.891	0.9037	0.8936
Design HP/IP/LP Shaft RPM	LP		HP
	4230		9850
Engine Total Mass	12 200 lb		

Table 2.2 KO-22/23 Summary table

2.5.1 Engine off-design analysis

Optimizing the engine to achieve the lowest TSFC and required Thrust at Supersonic Cruise is just the beginning . However, combined with off-design performance, whole project became much more complicated. The following summary tables show off-design performance.

2.6 Weight estimation

Weight estimation is based on equation 2.1 It is comparation of two engines. Comparing KO-22/23 to nowadays generation engines weight is 12 200lb. Bling and Blisk technologies allow to reduce mass approximately for 50%.

$$\frac{Weight}{Weight\_Ref} = \left(\frac{Wc}{Wc\_Ref}\right)^{1.1} * \left(\frac{Nstg}{Nstg\_Ref}\right)^{n}$$

Equation 2.1[2.1]

3. Inlet

Preliminary design calculations emerged two-dimensional single-duct inlet as the best solution for KO-22/23. All of most important issues was taken into consideration as weight, costs, manufacturing and especially total pressure recovery. The inlet at Mach 1.67 resulted 0.95 in a TPR and 1% of bleed of at the critical condition. The design sizing calculation was made as was proposed in RFP. Total inlet drag are estimated at 27835 lbf.

Location of inlet is consistent with NASA Final Report of Supersonic Civil Aviation for 2020 over the wings in the back of airplane[3.5].

To provide wide stability margin, low costs and low weight, which is approximately 4000 lb of same stress structure, the inlet is described as 2D mix compression configuration [.3.4]. Furthermore it is well known construction, it is used in the F-15, F-14 as well as in the Mig-29. The length of the axisymmetric inlet increase significantly. Maintenance is less complicated because inlet is one duct, there is direct access to fan and ramp servomotors. In case of mounting box with generators under the throat there would be well access as well. External compression elements incorporates two ramps to provide nearly isentropic free-stream compression (0.997; 0.998 static pressure loss to EX, and 0.993 to TH) prior to throat shock. First ramp is fixed and set to 5 deg. Second ramp is moveable and set to 6 degree in subcritical condition (Figure 3.1). The short diffuser length require some form of flow control devices like micro porous honeycomb composite materials to reduce potential for shock induced separation and energize diffuser flows[3.4]. It is calculated that bleeding valves have good influence on TPR [3.2], however, it takes some mass flow from main path. This air is implemented to second duct behind fan. To avoid suction of the boundary layer under the first ramp there is installed aerodynamically matched distributor. This issue is worth to be investigated in future because there could be a possibility to direct this mass of air straight to nozzle in order to reduce noise during take-off. On the other hand placement more curvature near inlet may cause the occurrence of oblique shocks, which may propagate to vertical tail.

3.1 Preliminary calculations

A_x/A_y	Value	Area	Value[ft2]	Mass flow	lb/s
A_{0des}/A_c	0.840	A_c	42.98	W_c	717.39
A_{obld}/A_c	0.010	A_0	36.75	W_0	613.37
A_{obyp}/A_c	0.015	A_{0byp}	0.645	W_{byp}	10.76
A_0/A_c	0.855	A_{bld}	0.430	W_{bld}	7.174
A_{spl}/A_c	0.135	A_{spill}	5.803	W_{spill}	96.85
A_{oi}/A_c	0.865	A_{oi}	37.18	W_{oi}	601.78
A_2/A_c	0.983	A_2	42.23	W_{eng}	602.61

Table 3.1 Main areas and mass flow

Factor	Value	Unit
eRam	0.952	-
C_{dspill}	0.01	-
C_{dbld}	0.018	-
C_{dbyp}	0.02	-
D	27835.2	lbf

Table 3.2 Drag factors and gross inlet drag

The path of calculations of inlet is based on points included in RPF chapter 5. The results of those calculations are all important for off-design. A description of matching operation is omitted in this report. Further calculations allow to design geometry and well predict TPR are shown below. Inlet should be designed for M_{local}=1.67 (Figure 3.3) when it is located over the wings.

EX		**T_h**		**Diff**			
M_{local}	1.67	A_{Th}/A_c	0.733	$2\phi_D$ [deg]	15	$p_{t2}/p_{t1\ NS}$	0.990
β_1 [deg]	41.63	A_{Th} [Ft^2]	31.48	α_{cowl} [deg]	3	p_{t2}/p_{th}	0.959
τ_1 [deg]	5	M_{th}	1.15	$\alpha_{cowltop}$ [deg]	3	p_{t2}/p_{thdiff}	0.953
Ma_{EX1}	1.516	M_{diff}	0.766	Y_o	0.10	V_2 [Ma]	0.550
Ma_{EX1n}	0.905			K_f	0.011	p_{t21}/p_{t11}	0.99974
β_2 [deg]	47.05			K_o	0.008	p_{t22}/p_{t12}	0.99859
τ_2 [deg]	6			K_m	1.220	p_{t2n}/p_{t1n}	0.99669
Ma_{2EX}	1.377			K_d	0.220	p_{t2f}/p_{t2n}	0.95651
Ma_{2EXn}	0.904					IPR	0.951

Table 3.3 Calculation results

3.2 Brief explanation of flow calculations

Pattern for design geometry and calculate external compression shocks is *Aircraft Propulsion 2-nd ed*. By Saeed Farokhi. First of all it is essential to select how many ramps would be installed in 2D inlet. It is proposed to install two ramps because this layout contains only one actuator. Three shocks has the same efficiency as 4 and more shock for 1.67 Ma. Oblique shocks created on ramps (focused compression) and on curvature between section L and 1 (distributed compression) are fall on cowl during supersonic condition. An Oswatitsch criterion is used to choose a proper ramp angle, when the shocks are of equal strength, $M_{1n}=M_{2n}$ The results are similar to Figure 3.1.

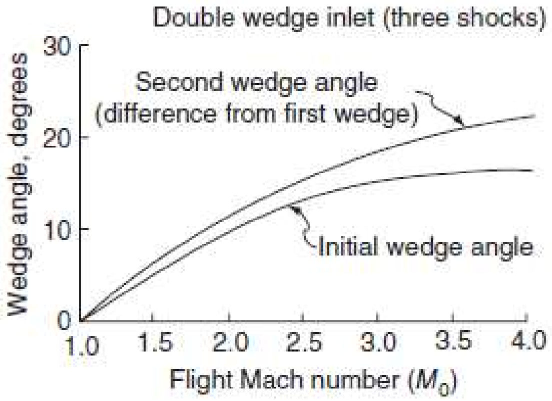

Figure 3.1 Wedge angle of Mach function[3.1]

It is desired to create a normal shock inside the inlet down the throat. The situation when normal shock moves to a cowl lip and even worse ahead the cowl lip is very undesirable. It cause magnified spillage and *Buzz*. A general rule is that M_{EX2} = 1.3 to avoid separation of the centrebody boundary layer at its interaction with the normal terminal shock. This Mach number might be larger but still must be smaller than the inflow Mach number, $M_{EX} < M_L$[3.3].

The cowl lip angles should align roughly to the angle of the flow at the cowl lip to minimize the generation of exterior shocks especially strong shocks. The cowl lip exterior angle should be 3-5 degrees greater than the interior angle to allow some structural bulk for the trialing edge[3.3].

The standard that address the shock recovery of supersonic inlets is MIL-E-5008B and provides 0,962 for flight Mach number M_0=1.6.

TPR calculated on 0.951 is not perfect but in this report fuselage drag are omitted. Those drugs decrease M_l to lower values than 1.67, thereby increasing TPR[Fig.3.3]. In this report calculation of inlet do not take into account those drugs and elliptic top surface of inlet (implemented). Otherwise TPR is estimated to be at least 0.962.

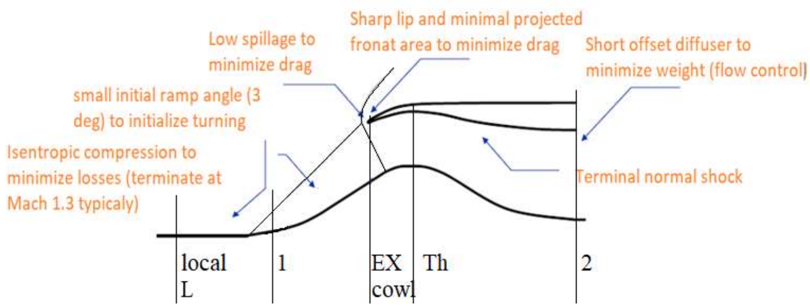

Figure 3.2 Inlet optimization scheme

TPR is very close to TPR which was calculated using CFD for similar inlet. That data was published in *SUPIN: A Computational Tool for Supersonic Inlet Design, John W.Slater.*[3.2]

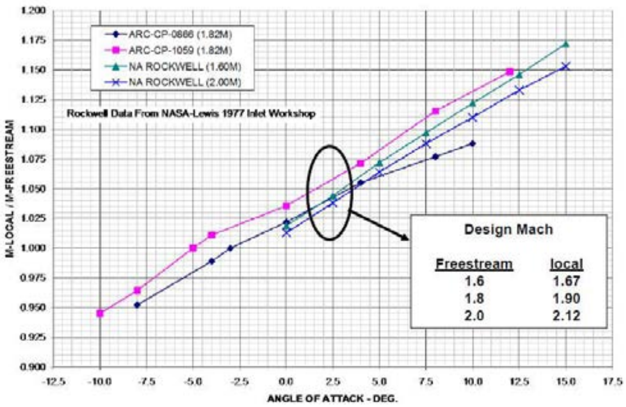

Figure 3.3 Over-wing Inlet design Mach[3.6]

3.3 Pressure loses

The surface of the diffuser is formed by tracing streamlines through the Busemann flow field. The process involves defining a tracing curve within the outflow and then integrating the streamlines in the upstream direction through the flow field. The tracing curve is a closed curve defined on a plane that is perpendicular to the flow. The tracing curve is built of separate super-ellipses for the top and bottom. The paper by Konscek presents one of the earliest applications of the super-ellipse for inlet design [3.3].

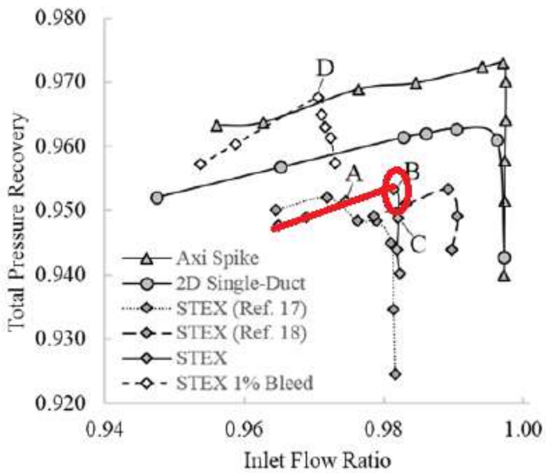

Figure 3.4 Characteristic “cane” curve for the Mach 1.6[3.2].

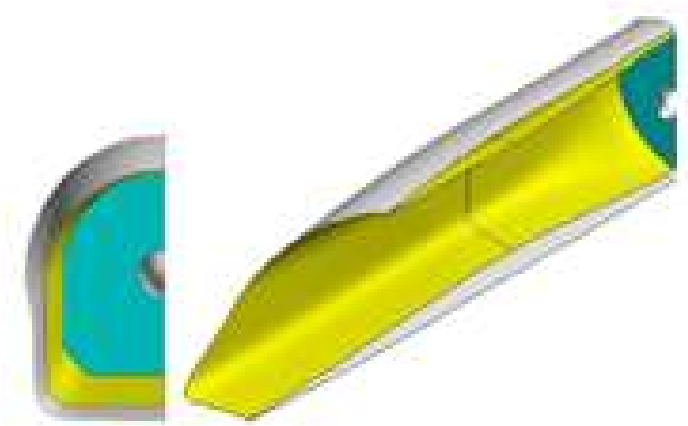

Figure 3.5 Example of streamline-traced inlet with tracing curves[3.3]

Furthermore, an elliptic top edge decrease irregular flow in intake. The problem is due to vortices arising in curved structures. It is not a well-researched phenomenon.

All of subsonic diffuser factors are taken from Inlet Performance Analysis Code Paul J. Barnhart. To begin with Kd-empirical subsonic diffuser total pressure loss factor (most effective $2\phi_D$ angle is 10 deg., which makes diffusor very long, so great compromise is 16 deg.

K_f-empirical subsonic diffuser friction loss factor

K_m-empirical subsonic diffuser throat Mach number factor

K_o-empirical off-set loss factor

A diffusor is designed to achieve a value of $Y_0 \sim 0$.

$$K_D = f(2\theta_D)$$

$$K_O \simeq 1.2\left(\frac{Y_O}{L_D}\right)$$

$$K_F = 4f_D\left(\frac{L_D}{D_2}\right)$$

$$f_D \simeq 0.0025$$

$$K_M = f(M_{TH})$$

Equation 3.4 Pressure loss factor for subsonic diffusor[3.7]

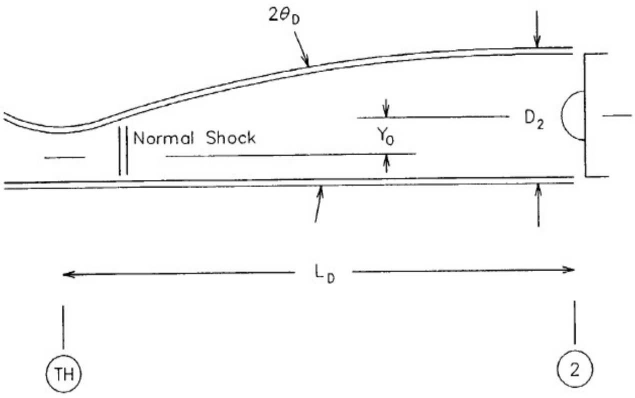

Figure 3.6 Subsonic diffusion modeling elements[3.7]

$$\frac{P_{T2}}{P_{T0}} = \left(\frac{P_{TL}}{P_{T0}}\right)\left(\frac{P_{T1}}{P_{TL}}\right)\left(\frac{P_{TTH}}{P_{T1}}\right)\left(\frac{P_{T2}}{P_{TTH}}\right)$$

Equation 3.5 Equation of TPR[3.7]

3.4 Geometry

At the figure 3.7 and 3.8 there are schematic shames of inlets. In the table 3.4 there are collected all important values related with dimensions of inlet. It is included to show the simplicity of the design and its originality. Orange color marks short diffusor dimension whereas blue total length of inlet.

The geometry of KO-22/23's inlet fully corresponds with flow properties. Few general targets are harvested below:

a) Meet high performance on cruise condition
b) Achieve no-bleed flow or though 1% to stabilize flow
c) Length of ramps is caused by oblique shocks, length of diffusor is determined by $2\phi_D$ angle and reduction of velocity Mth
to M2.
d) Minimize all factor associated with diffusor losses. Minimize Y_0, $2\phi_D$, L_d.
e) Minimize mass and cost of manufacturing and maintenance.

	Value[ft]	x/D2						
L_{cowl}	6.647	0.9	L_{r1}	1.1477	H_{req1}	3.412	$H_{ell\ Th}$	2.505
L_{cowl}-T_h	3.747	0.51	Wid_1	8	A_{req}/A_c	0.635	$H_{req\ Th}$	1.968
L_{Th-2}	7.993	1.08	H_1	5.908	Wid_2	8	H_{Th}	6.008
L_c	18.389	2.48	H_{ell1}	2.495	$A_{ell\ Th}/A_c$	0.5	h_{Th}	1.53

Table 3.4 Table 3.4 Geometric dimensions of the inlet

In supersonic issues great attention is placed to noise reduction. Even factoring in the projection of 3-dB effective perceived noise level (EPNL) reduction from proposed *Low Noise Fan*[3.5] To achieve noise reduction goals which are firm requirements for the HSCT most of inlets must have increase length. Additional treatment area was found in the 2D inlet such that an increase in its length was not required. What is more there are many advantages of placement engine over wings. Sound waves are reflecting from the ramps and wings straight to space. It solves a problem of swirl which sucks dirt from the ground.

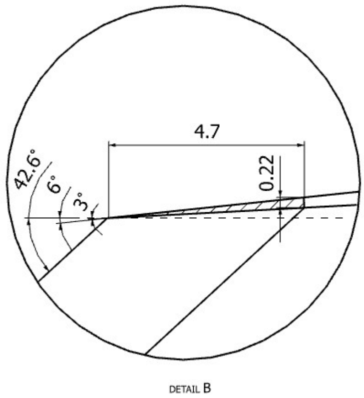

Figure 3. 8 Titanium front edge[in]

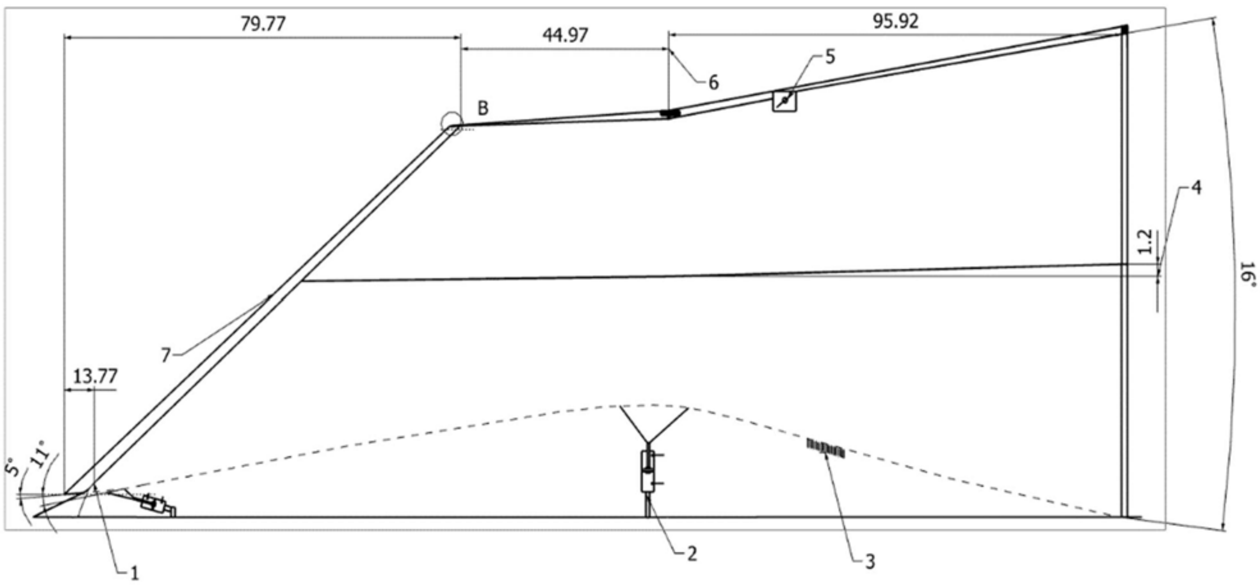

Figure 3.7 Shame of inlet; 1. Moveable second ramp with servomotor, 2. Control system for the throat section, 3. Micro-scale composite bleed vanes, 4. Minimized difference between the fan axis and the middle of the throat, 5. Bypass door, 6. Reinforced Titanium rib

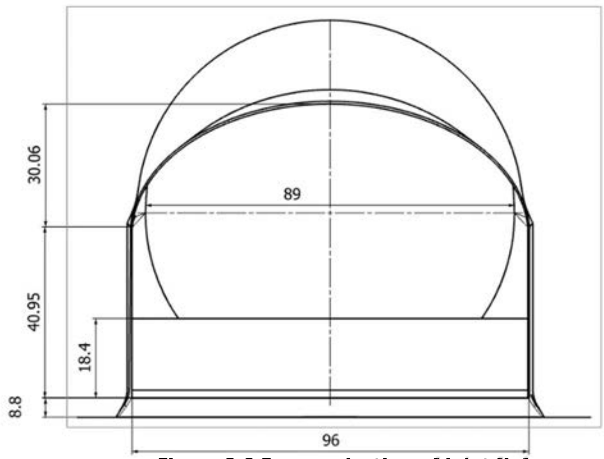

Figure 3.9 Face projection of inlet [in]

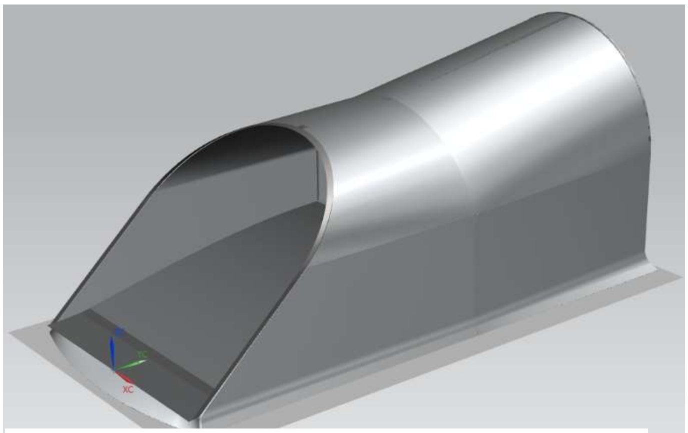

Figure 3.10 3D model of designed KO-21/22 inlet

3.4.1 Material and executive system

Main material to produce such inlet could be Aluminum 2014 and Titanium Ti-6Al-4V for stiffening elements. Those elements should be located where the shocks occur and along the inlet axis. Another part made of Titanium must be a frontal edge of inlet. Mass of inlet is estimated at 4000 lb.

An upper elliptic part is one-piece of metal what is made it easy to manufacturing. It may be built of just a few components because width and length is the same in section 1 and Th. In the same way second part of this sections may be manufactured with few components. The structure of inlet should be fixed to fuselage.

All curvature connecting inlet and fuselage must be bent. Despite the hardship of produce such structure it is essential to reduce interfered drag.

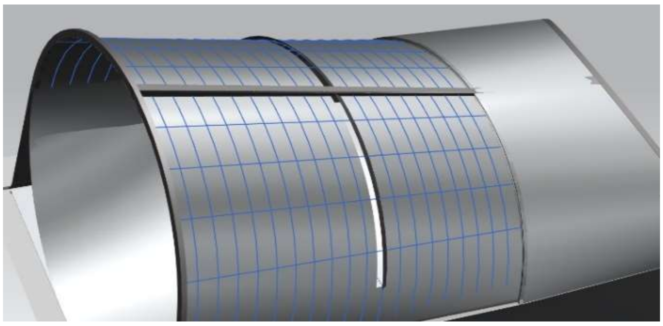

Figure 3.11 View of stiffening elements

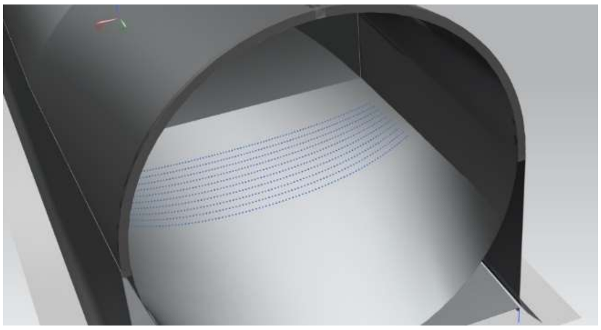

Figure 3.12 View of bleed vanes

Area between bleed vanes and fan is lined with screen that absorbs noise. Blue net symbolizes reinforced hull inlet at the Figure and bleed vanes at Figure. While notch is bypass door which drain air to second duct.

Inlet executive system contains just two servomotors. One is to control second ramp angle, and the other controls throat area. Two sheet metal parts of the throat are not connected to each other that which is inseparable with second ramp cover another. This allows moving the flaps freely and preventing leaks. System could be supplied with oil from the main tank. In case of wire break in general district this oil may be used to another more important sections. Cowl lip is not movable because a solution with elliptic top edge was chosen. Furthermore another servomotor increase mass, maintenance complication and thickening inlet cover.

3.5 Anti-icing system

Consequences of ice in inlet or fan blade are disturbed flow which may lead to unsteady work of compressor or detached ice formation may even damage blades. To avoid such negative influence of ice, which may appear during a flight on structural parts of plane and engine are applied some kind of anti-icing system. In KO-22/23 it would be solved in the following way. From the fourth stage of compressor would be taken 1% of air mass flow which have around 954°R and would be used to warm nose cap. Also due to the fact that there is not so much space on edges of inlet to use air for warming it was decided to make it by electric system – the heating pads. The same system would be used to an inlet quid vane and bottom inlet ramp. Since engines would be placed on the wings and ice formation may settle there and after some time detach and damage engine is advised to put such heating pads in front of inlet.[39]

4. COMPRESSOR DESIGN

This chapter contains calculations of velocity triangles and geometry blades, stage-by-stage analysis of parameters, 3-D compressor design and analysis of material selections. To start the design process the specific parameters like static and total pressure, static and total temperature, fan, LP and HP pressure ratio, mass flow are needed and are calculate by GasTurb. The shafts speed is selected based on the design choice of tip speed which is 1 642.32 ft/s. It can be so high because the compressor consists of blisk and bling technology, which also reduces mass by 30% [4.8].

For the stage-by-stage analysis of parameters and calculations of velocity triangles the calculations were carried out for three different radiuses for each stage. For the correct results we used inlet guide vanes, because the swirl before the inlet to the fan is 204.19 ft/s.

To avoid separation of airflow from the blade whole process of blade design was determined D-Factor which values should be around 0.6 and in calculations of compressors are around 0.51.

4.1 FAN DESIGN

4.1.1 Inlet Fan Flow Parameters

The total/static pressure and temperature and mass flow rate are given by GasTurb analysis. All of them are detailed in the table 4.1.

Parameters	Value
Static pressure [Psi]	11.98
Total pressure[Psi]	14.7
Static temperature [°R]	489.23
Total temperature [°R]	518.67
Density[lb/ft^3]	0.07

Table 4.18 Parameters specified in GasTurb

The values of inner and outer radius are given, so we can compute the pitch one, by using the equation: $r_m = \sqrt{\frac{r_t{}^2+r_h{}^2}{2}}$

Parameters	Value
Radius tip [in]	44.49
Radius pitch [in]	28.92
Radius hub [in]	13.35
Area [in^2]	5657.51

Table 4.19 Geometric parameters of fan

4.1.2 Fan exit flow parameters

Due to the fact that compression is determined as a polytrophic process, it is used patterns:

$$p_2{}^* = \prod_s{}^* * p_1{}^*$$

$$T_2{}^* = T_1{}^*(1 + \frac{(\prod_s{}^*)^{\frac{k-1}{k}} - 1}{\eta_s{}^*})$$

We based our data from GasTurb and the pressure ratio fan is 1.99.

Parameters	Value
Static pressure [Psi]	14.42
Total pressure [Psi]	20.77
Static temperature [°R]	551.16
Total temperature [°R]	579.14
Density [lb/ft^3]	0.11

Table 4.20 Parameter specified in GasTurb

When it comes to geometry, the main output pattern was the continuity equation which allows to count the area for each stage.

$$\dot{m} = A\rho C$$

An important point in the design of the compressor was the assumption that the hub radius is constant.

Parameters	Value
Radius tip [in]	44.49
Radius mean [in]	33.37
Radius hub [in]	22.24
Area $[in^2]$	2718.16

Table 4.21 Geometric parameters of fan

4.1.3 Shaft RPM

The rotational speed of the shaft is 4230 RPM. The reason for this is the need for high tip speed which is 1 642.32 ft/s to create good compressor working conditions and to achieve supersonic profiles. Ultimately the Mach number tip is 1.48.

4.1.4 Stage-by-stage analysis

For the fan design, it is significant to calculate stage-by-stage analysis for three different radius of blade. This process ensures regular growth of temperature and pressure. The calculations show that the fan has two stages.

4.1.5 The velocity triangles

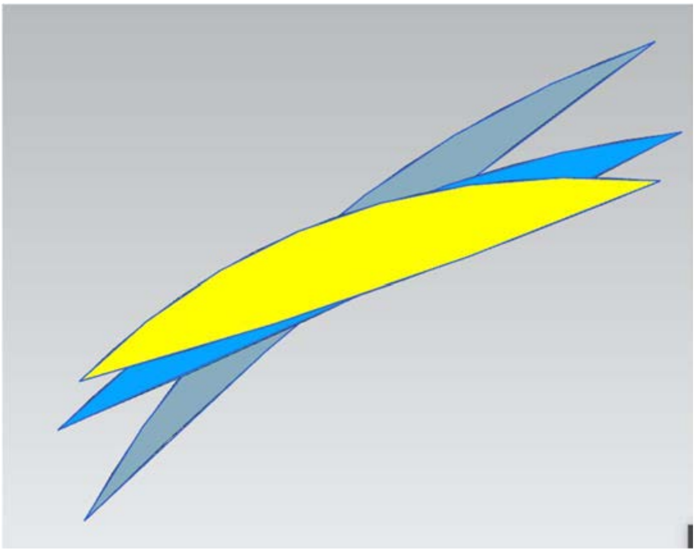

Figure 4.1 Ko-22/23 HPC I- stage blade airfoils hub to tip

The design begins with the velocity triangles from medium radius and the fact that the angle of swirl is $\alpha_1 = 20^{\circ}$, then using patterns with peripheral speed, axial velocity and trigonometric effects it is computed the other angles.

$$tan\alpha_2 = \frac{\Delta T * Cp}{U * C_x}$$

$$tan\beta_2 = \frac{-U}{C_x}$$

$$tan\beta_1 - tan\beta_2 = tan\alpha_2 - tan\alpha_1$$

The condition that we must fulfill in the course of these calculations is the de Haller criterion.

$$\frac{W_2}{W_1} > 0,7$$

4.1.6 The velocity of rotor.

Based on the book "Napędy lotnicze- Zespoły Wirnikowe Silników Turbinowych"- Z. Dżygadło, is founded the axial velocities C_x are constant along blade on first stage from 524.93 to 721.78 ft/s.

$C_{1u} = C_{1x} * tan\alpha_1$, $C_1 = \sqrt{C_{1x}{}^2 + C_{1u}{}^2}$, $U_1 = \frac{\Pi * D * N}{60}$, $W_{1u} = C_{1u} - U_1$, $W_1 = \sqrt{C_{1x}{}^2 + W_{1u}{}^2}$, $C_{2u} = C_{2x} * tan\alpha_2$, $C_2 = \sqrt{C_{2x}{}^2 + C_{2u}{}^2}$, $U_2 = U_1$, $W_{2u} + C_{2u} - U_2$, $W_2 = \sqrt{C_{2x}{}^2 + W_{2u}{}^2}$

4.1.7 The velocity of stator.

$C_{3u} = C_{3x} * tan\alpha_3$, $C_3 = \sqrt{C_{3x}{}^2 + C_{3u}{}^2}$, $U_3 = U_2$, $W_{3u} = C_{3u} - U_3$, $W_3 = \sqrt{C_{3x}{}^2 + W_{3u}{}^2}$

4.1.8 Results

	I Fan stage	II Fan Stage	I Fan stage	II Fan Stage	I Fan stage	II Fan Stage
C1 [ft/s]	756.1	771.8	631.8	678.6	610.1	642.8
C1a[ft/s]	593.7	593.7	593.7	593.7	593.7	593.7
C1u[ft/s]	-468.2	493.2	-216.1	328.8	-140.5	246.6
W1[ft/s]	1129.8	678.1	1413.9	1080.4	1878.6	1516.4
W1u[ft/s]	-960.7	-327.7	-1283.3	-902.6	-1782.4	-1395.4
U1[ft/s]	492.6	820.9	1067.2	1231.4	1641.9	1641.9
Alfa1[deg]	-38	40	-20	29	-13	23
Beta1[deg]	-58	-29	-65	-57	-72	-67
C2[ft/s]	240.7	1244	640.4	939.9	613.9	806.9
C2a[ft/s]	593.7	593.7	593.7	593.7	593.7	593.7
C2u[ft/s]	520.4	1093.2	240.2	728.8	156.1	546.6
W2[ft/s]	594.3	653.2	1018.1	777.9	1600	1245.9
W2u[ft/s]	27.8	272.3	827.1	502.6	1485.8	1095.3
U2[ft/s]	934.47	652.53	1288.4	1147.43	1642.33	1642.33
Alfa2[deg]	41	61	47	51	34	43
Beta2[deg]	-3	-25	-37	-40	-68	-62

Table 4.22 The velocity triangles on hub, pitch and tip radius

4.2 LOW PRESSURE COMPRESSOR DESIGN

4.2.1. Inlet flow low pressure compressor parameters

The total/static pressure and temperature and mass flow rate are given by GasTurb analysis the pressure ratio LPC is 1.12. All of them are detailed in the table 4.6.

Parameters	Value
Static pressure [Psi]	25.32
Total pressure[Psi]	28.9
Static temperature[°R]	62
Total temperature[°R]	64.38
Density[lb/ft^3]	0.11

Table 4.23 Parameter specified in GasTurb

All of the calculations are made on the basis of the same formulas as fan design.

Parameters	Value
Radius tip[in]	33.38
Radius mean[in]	30.66
Radius hub[in]	27.94
Area[in^2]	1047.19

Table 4.24 Geometric parameters of low pressure compressor

4.2.2 Exit flow low pressure compressor parameters

Parameters	Value
Static pressure[Psi]	28.99
Total pressure[Psi]	32.41
Static temperature[°R]	64.46
Total temperature[°R]	66.54
Density[lb/ft^3]	0.12

Table 4.25 Parameter specified in GasTurb

Parameters	Value
Radius tip[in]	33.38
Radius mean[in]	30.66
Radius hub[in]	27.94
Area[in^2]	1016.94

Table 4.26 Geometric parameters of low pressure compressor

4.2.3 Shaft RPM

The rotational speed of the shaft is the same like fan- 4230 RPM. The reason for this is that both fan and low pressure compressor work on the same shaft.

4.2.4 Stage-by-stage analysis

As in case of fan design, it is significant to calculate stage-by-stage analysis for three different radius of blade. This process ensures regular growth of temperature and pressure. The calculations show that the LPC has one stage.

4.2.5 The velocity triangles

To calculate the speed on each subsequent step we assumed that C_{3u} on the first stage is C_{1u} on the second stage and C_{3x} on the first stage is C_{1x} on the second stage. When we passed from fan to low pressures compressor the C_{3u} on the last stage is C_{1u} on the first stage and C_{3x} on the last stage is C_{1x} on the first stage. Rest of the velocities and angles are counted from the same patterns.

4.2.6 Results

	I LPC	I LPC	I LPC
C1[ft/s]	621.9	617.2	613.6
C1a[ft/s]	593.6	593.6	593.6
C1u[ft/s]	185.4	168.9	155.2
W1[ft/s]	1033.5	1130.9	1229.5
W1u[ft/s]	-845.9	-962.6	-1076.7
U1[ft/s]	1031.3	1131.6	1231.9
Alfa1[deg]	17	16	15
Beta1[deg]	-55	-58	-61
C2[ft/s]	754.2	729.5	709.9
C2a[ft/s]	593.7	593.7	593.7
C2u[ft/s]	465.1	423.9	389.4
W2[ft/s]	820.4	814.3	1030.7
W2u[ft/s]	566.2	707.7	842.5
U2[ft/s]	1037.88	1135.03	1232.19
Alfa2[deg]	38	50	33
Beta2[deg]	-44	-36	-55

Table 4.27 The velocity triangles on hub, pitch and tip radius

4.3 HIGH PRESSURE COMPRESSOR DESIGN

4.3.1 Inlet flow high pressure compressor parameters

The total/static pressure and temperature and mass flow rate are given by GasTurb analysis the pressure ratio fan is 13.37. All of them are detailed in the table 4.11 .

Parameters	Value
Static pressure[Psi]	26.99
Total pressure[Psi]	32.08
Static temperature[°R]	633.51
Total temperature[°R]	665.44
Density[lb/ft^3]	0.11

Table 4.28 Parameters specified in GasTurb

All of the calculations are made on the basis of the same formulas as fan and LPC design.

Parameters	Value
Radius tip[in]	19.18
Radius mean[in]	14.38
Radius hub[in]	9.58
Area[in^2]	866.39

Table 4.29 Geometric parameters of high pressure compressor

4.3.2 Exit flow high pressures compressor parameters

Parameters	Value
Static pressure[Psi]	34.38
Total pressure[Psi]	40.61
Static temperature[°R]	679.45
Total temperature[°R]	712.43
Density[lb/ft^3]	0.73

Table 4.30 Parameters specified in GasTurb

Parameters	Value
Radius tip[in]	19.18
Radius mean[in]	18.8
Radius hub[in]	18.42
Area[in^2]	116.99

Table 4.31 Geometric parameters of high pressure compressor

4.3.3 Shaft RPM

The rotational speed of the shaft is 9850 RPM.

4.3.4 Stage-by-stage analysis

As in case of fan and LPC design it is significant to calculate stage-by-stage analysis for three different radius of blade. This process ensures regular growth of temperature and pressure. The calculations show that the HPC has eleven stages.

4.3.5 The velocity triangles

To calculate the speed on each subsequent step we assumed that C_{3u} on the first stage is C_{1u} on the second stage and C_{3x} on the first stage is C_{1x} on the second stage. When we passed from fan to low pressures compressor the C_{3u} on the last stage is C_{1u} on the first stage and C_{3x} on the last stage is C_{1x} on the first stage. Rest of the velocities and angles are counted from the same patterns.

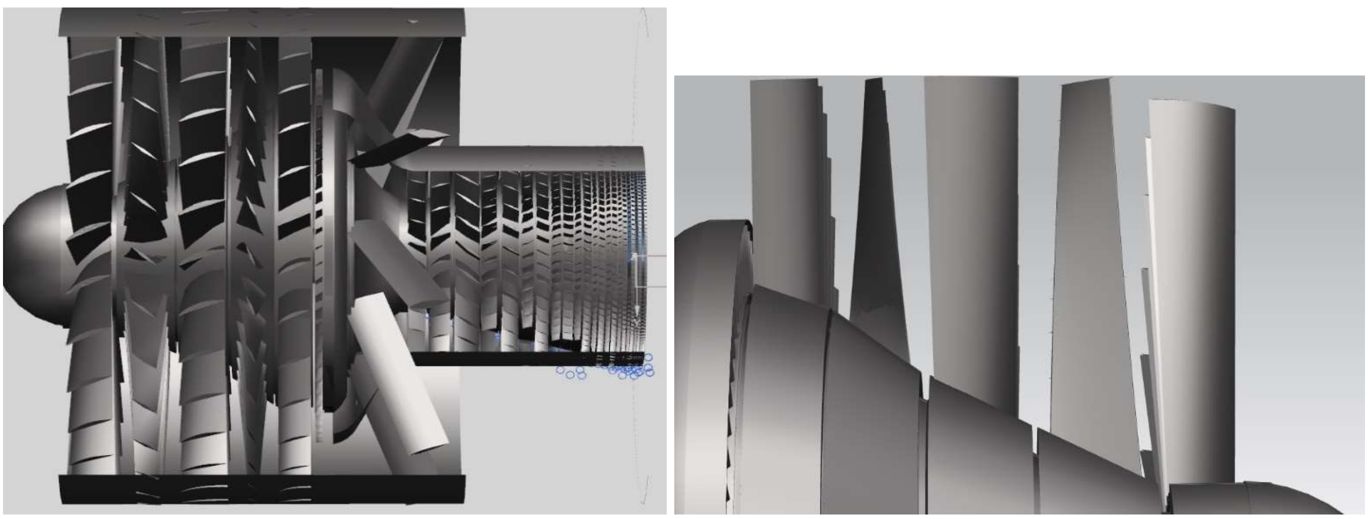

Figure 4.3-D model of compressor and fan and the blade of compressor

Figure 4.4 The blade of compressor

4.3.6 Results

	I HPC	II HPC	III HPC	IV HPC	V HPC	VI HPC	VII HPC	VIII HPC	IX HPC	X HPC	XI HPC
C1[ft/s]	609.6	590.2	579	556.6	551.9	537.8	522.5	507.6	492.4	477.1	472.1
C1a[ft/s]	593.7	577.3	560.9	535.8	528.1	511.7	495.3	478.9	462.5	446.1	429.7
C1u[ft/s]	138.4	122.9	143.6	150.7	160.3	165.4	166.4	168.4	169.1	169.2	195.7
W1[ft/s]	906.9	1076.8	1205.9	1260.7	1345	1396.7	1415.1	1442.6	1459.1	1469.9	1452.7
W1u[ft/s]	-685.6	-909	-1067.6	-1141.2	-1237	-1299.6	-1325.6	-1360.8	-1383.8	-1400.7	-1387.7
U1[ft/s]	823.9	1031.9	1211.2	1291.9	1397.3	1465	1492	1529.2	1552.9	1569.8	1583.4
Alfa1[deg]	7	12	14	16	17	18	19	19	20	21	24
Beta1[deg]	-49	-58	-62	-65	-67	-69	-70	-71	-72	-72	-73
C2[ft/s]	905.2	837.3	788.1	755.2	725.8	698.9	676.1	652.4	629.8	607.8	585.8
C2a[ft/s]	593.7	577.3	560.9	544.5	528.1	511.7	495.3	478.9	462.5	446.1	429.7
C2u[ft/s]	683.3	606.4	553.6	5233	497.9	476	460	443	427.5	412.8	398.2
W2[ft/s]	610.1	717.1	864.3	959	1043	1113.4	1144.5	1187.1	1216.7	1240.1	1260.7
W2u[ft/s]	140.7	425.5	657.6	789.4	899.4	988.9	1031.8	1086.2	1125.4	1157.1	1185.2
U2[ft/s]	930.6	1116.8	1252.1	1363.8	1424.7	1472.1	1509.3	1536.4	1556.7	1577	1587.2
Alfa2[deg]	49	46	45	44	43	43	43	43	43	43	43
Beta2[deg]	-13	-36	-50	-55	-60	-63	-64	-66	-68	-69	-70

Table 4.32 The velocity triangles on hub radius

	I HPC	II HPC	III HPC	IV HPC	V HPC	VI HPC	VII HPC	VIII HPC	IX HPC	X HPC	XI HPC
C1[ft/s]	600.8	584.9	578.9	552.3	551.9	537.7	522.9	507.4	492.4	477.1	472.1
C1a[ft/s]	593.6	577.2	560.8	535.8	528.1	511.7	495.3	478.9	462.5	446.1	429.7
C1u[ft/s]	92.3	94.6	121.7	133.7	147.1	155.7	158.1	162.1	164.1	165.1	191.7
W1[ft/s]	1288.6	1372.6	1423	1427.6	1473.4	1491.3	1496.2	1504.7	1508.9	1511.1	1487.3
W1u[ft/s]	-1143.7	-1245.3	-1307.9	-1323.2	-1375.5	-1400.8	-1411.8	-1426.4	-1436.3	-1443.8	-1423.8
U1[ft/s]	1235.9	1339.9	1429.5	1456.8	1522.5	1556.4	1569.9	1588.5	1600.4	1608.8	1615.6
Alfa1[deg]	13	12	14	16	17	18	19	19	20	21	24
Beta1[deg]	-63	-65	-67	-68	-69	-70	-71	-71	-72	-73	-73
C2[ft/s]	748.3	742.5	731.2	715.4	6983	680.1	6608	641.3	621.3	600.7	580.4
C2a[ft/s]	593.7	577.3	560.9	544.5	528.1	511.7	495.3	478.9	462.5	446.1	429.6
C2u[ft/s]	455.5	467	469.1	464.1	456.9	448.1	437.4	426.5	414.9	402.8	390.2
W2[ft/s]	927.8	988.2	1024.6	1044.4	1060.8	1073.7	1077.2	1083.3	1086	1088	1070.8
W2u[ft/s]	780.4	872.9	960.5	1016.2	1065.7	1108.4	1132.6	1162.1	1185.6	1206.1	1225.4
U2[ft/s]	1289.45	1382.5	1450.23	1506	1536.5	1560.2	1578.79	1592.33	1602.48	1612.63	1617.71
Alfa2[deg]	55	61	63	66	67	69	70	71	72	73	73
Beta2[deg]	-33	-30	-29	-28	-26	-25	-25	-24	-23	-22	-22

Table 4.33 The velocity triangles on pitch radius

	I HPC	II HPC	III HPC	IV HPC	V HPC	VI HPC	VII HPC	VIII HPC	IX HPC	X HPC	XI HPC
C1[ft/s]	597.7	582.4	570.7	549.1	545.3	532.4	517.7	503.7	489.2	474.3	469
C1a[ft/s]	593.7	577.3	560.9	535.9	528.1	511.7	495.3	478.9	462.5	446.1	429.6
C1u[ft/s]	69.2	76.9	105.6	120.1	135.9	147	150.7	156.3	159.4	161.2	188
W1[ft/s]	1686.6	1673.7	1641.1	1594.5	1601.6	1585.7	1577	1566.6	1558.7	1552.2	1521.8
W1u[ft/s]	-1578.7	-1570.9	-1542.3	-1501.7	-1511.9	-1500.8	-1497.2	-1491.6	-1488.5	-1486.8	-1459.9
U1[ft/s]	1647.9	1647.9	1647.9	1621.8	1647.9	1647.9	1647.9	1647.9	1647.9	1647.9	1647.9
Alfa1[deg]	7	8	11	13	14	16	17	18	19	20	24
Beta1[deg]	-69	-70	-70	-70	-71	-71	-72	-72	-73	-73	-74
C2[ft/s]	684.9	690.9	692.9	685.7	676.1	664	647.2	631.2	613.4	594.6	575.3
C2a[ft/s]	593.7	577.3	560.9	544.5	528.1	511.7	495.3	478.9	462.5	446.1	429.6
C2u[ft/s]	341.6	379.7	406.9	416.9	422.2	423.2	416.7	411.1	402.9	393.2	382.6
W2[ft/s]	1434.8	1393.3	1361.8	1346.1	1334.7	1327.3	1327.1	1326.2	1328.1	1331.6	1336.3
W2u[ft/s]	1306.2	1268.1	1240.9	1231	1225.7	1224.7	1231.2	1236.7	1244.9	1254.6	1265.3
U2[ft/s]	1648.3	1648.3	1648.3	1648.3	1648.3	1648.3	1648.3	1648.3	1648.3	1648.3	1648.3
Alfa2[deg]	30	33	36	37	39	40	40	41	41	41	42
Beta2[deg]	-66	-66	-66	-66	-67	-67	-68	-69	-70	-70	-72

Table 4.34 The velocity triangles on tip radius

	I FAN	II FAN	I LPC	I HPC	II HPC	III HPC	IV HPC	V HPC	VI HPC	VII HPC	VIII HPC	IX HPC	X HPC	XI HPC
Pressure ratio stages	1.41	1.41	1.12	1.26	1.26	1.26	1.26	1.26	1.26	1.26	1.26	1.26	1.26	1.26
D-factor	0.61	0.6	0.61	0.61	0.61	0.61	0.61	0.61	0.61	0.61	0.61	0.61	0.61	0.61
De Haller	0.72	0.72	0.72	0.72	0.72	0.72	0.72	0.72	0.72	0.72	0.72	0.72	0.72	0.72
Work coefficient	0.32	0.27	0.1	0.18	0.17	0.16	0.16	0.16	0.16	0.17	0.18	0.19	0.2	0.21
Flow coefficient	0.55	0.48	0.52	0.48	0.43	0.39	0.37	0.35	0.33	0.32	0.3	0.29	0.28	0.27
$\frac{\boldsymbol{Hub}}{\boldsymbol{Tip}}$ ***Ratio***	0.3	0.5	0.84	0.5	0.63	0.74	0.8	0.85	0.89	0.9	0.93	0.94	0.95	0.96
Number of Blades	18	25	65	20	29	46	72	80	86	93	115	134	152	169
Blade chord [in]	7.7	5.5	1.35	2.85	2.9	2.11	1.66	1.27	0.95	0.83	0.64	0.52	0.44	0.37
Aspect Ratio	4.04	4.04	4.04	3.36	2.46	2.4	2.35	2.29	2.24	2.2	2.14	2.1	2.06	2.02
Taper Ratio	1	0.9	0.9	0.9	0.9	0.95	0.95	0.95	0.95	0.95	0.95	1	1	1
Degree of Reaction	0.6	0.6	0.8	0.8	0.8	0.8	0.8	0.8	0.8	0.8	0.8	0.8	0.8	0.8
Mach Number (absolute)	0.58	0.63	0.51	0.49	0.46	0.44	0.41	0.39	0.37	0.34	0.32	0.3	0.28	0.27
Mach Number (relative)	1.3	0.99	0.93	1.05	1.08	1.09	1.07	1.05	1.02	0.99	0.96	0.93	0.9	0.86

Table 4.18 Parameters on pitch for compressors

4.4 Blade material analysis

An important point in the design of the compressor is the selection of the right material from which it will be made. In mainly depends on the temperature which show table 4.18. It is very high and not all metals can work in this way and it affects the strength properties of construction materials and value of stress resulting from the occurrence of temperature gradients in the engine.

Parameters	**Values**
$T_1{}^*fan$	518.67 [°R]
$T_2{}^*fan$	643.79 [°R]
$T_1{}^*LPC$	643.79 [°R]
$T_2{}^*LPC$	665.42 [°R]
$T_1{}^*HPC$	665.42 [°R]
$T_2{}^*HPC$	1465.74 [°R]

Table 4.19 Parametric of temperature in fan. LPC and HPC

Citing the figure 4.2 of the material used will be SiC/SiC composite. It is the strongest material which can work in our the highest temperature 1 465.74R and also glass-ceramics density is low, 0.0505 $\frac{lb}{in^3}$, so that composite density is low. [4.7]

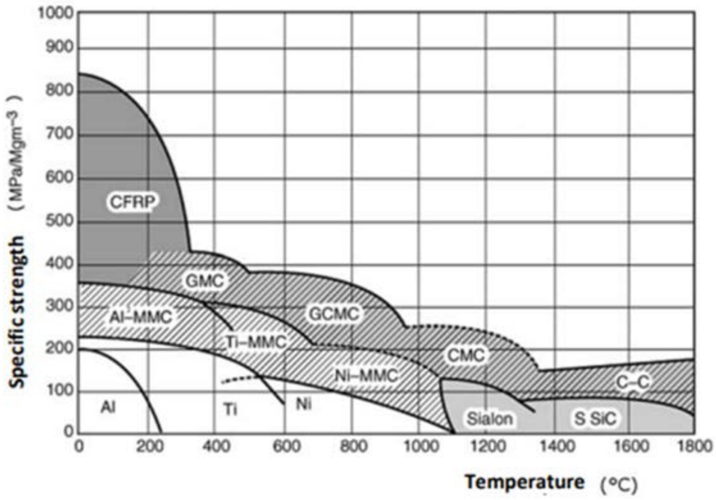

Figure 4.5 Specific strength depending on temperature [4.6]

The value of rotational speed affects the amount of centrifugal force acting on the rotor and very important is its relation with pressure, because it affects the value of longitudinal forces loading the rotor and its supports.

Blades are counted from bending strength of the pattern:

$$\sigma(R) = \rho * \omega^2 * \frac{{R_z}^2 - R^2}{2}$$

Discs are counted from[4.1]:

- ✓ strain from mass forces:
  - Radial $\sigma_r = \frac{3+\vartheta}{8} * \rho * U^2 * [1 - (\frac{r}{R})^2]$
  - Peripheral $\sigma_u = \frac{3+\vartheta}{8} * \rho * U^2 * [1 - \frac{1+3*\vartheta}{3+\vartheta} * (\frac{r}{R})^2]$
- ✓ Coronary loads
  - If disc is without hole $\sigma_r = \sigma_u = \sigma_w$
  - Radial $\sigma_r = \frac{\sigma_w}{1-(\frac{R_o}{R})^2} * [1 - (\frac{R_o}{r})^2]$
  - Peripheral $\sigma_u = \frac{\sigma_w}{1-(\frac{R_o}{R})^2} * [1 + (\frac{R_o}{r})^2]$
- ✓ Uneven heating
  - Radial $\sigma_r = \frac{\beta*\epsilon*T_w}{3} * \frac{1}{R} * \{\frac{R^3-{R_o}^3}{R^2-{R_o}^2} * [1 - (\frac{R_o}{r})^2] - \frac{r^3-{R_o}^3}{r^2}\}$
  - Peripheral $\sigma_u = \frac{\beta*\epsilon*T_w}{3} * \frac{1}{R} * \{\frac{R^3-{R_o}^3}{R^2-{R_o}^2} * [1 - (\frac{R_o}{r})^2] - \frac{r^3-{R_o}^3}{r^2} - 3 * r\}$

4.4.1 Construction of compressors

To obtain the smallest mass: fan, LPC and HPC, it was decided to use bling, which is a monolithic bladed ring forming one rotor stage of the compressor, and blisk technology. They are seam welding with hollow blade in which is stiffening truss. Their advantages are: increasing maximal speed of the rotor and significantly reducing mass. Except that we decided to use adjustable trailing edges of the fan blades in order to optimum work in all conditions and all blades of compressors would be make of SiC/SiC composite but on the leading edge will be titanium plates to prevent foreign object damage. The compressors use labyrinth seal to avoid backflow of airstream and to limit losses of pressures. The high pressure compressor is designed with three supports on III and XI stage for reducing distance between them in order to achieve higher rotational speed and rings are with balancing hole.

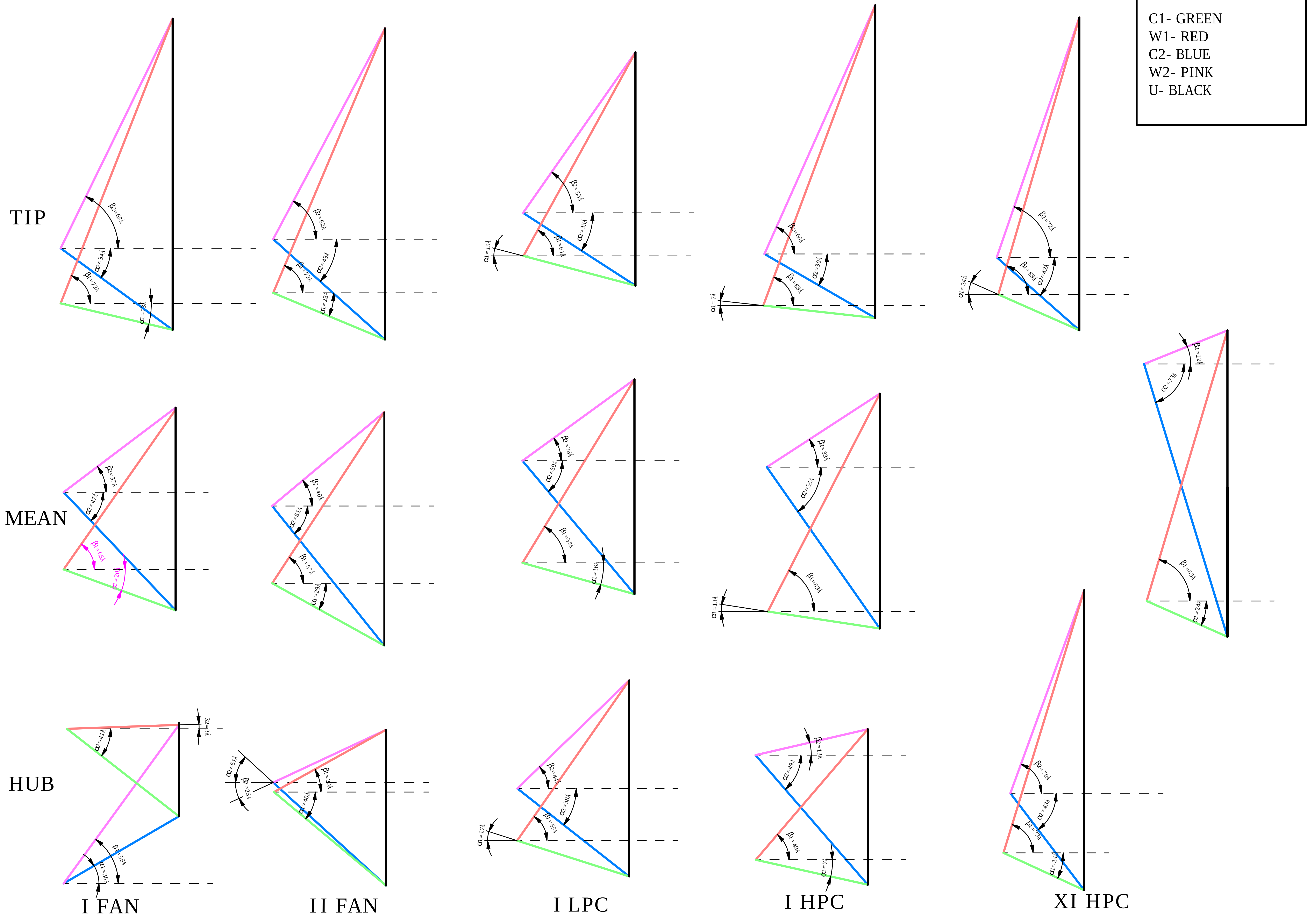
C1- GREEN
W1- RED
C2- BLUE
W2- PINK
U- BLACK
TIP
MEAN
HUB
I FAN
II FAN
I LPC
I HPC
XI HPC

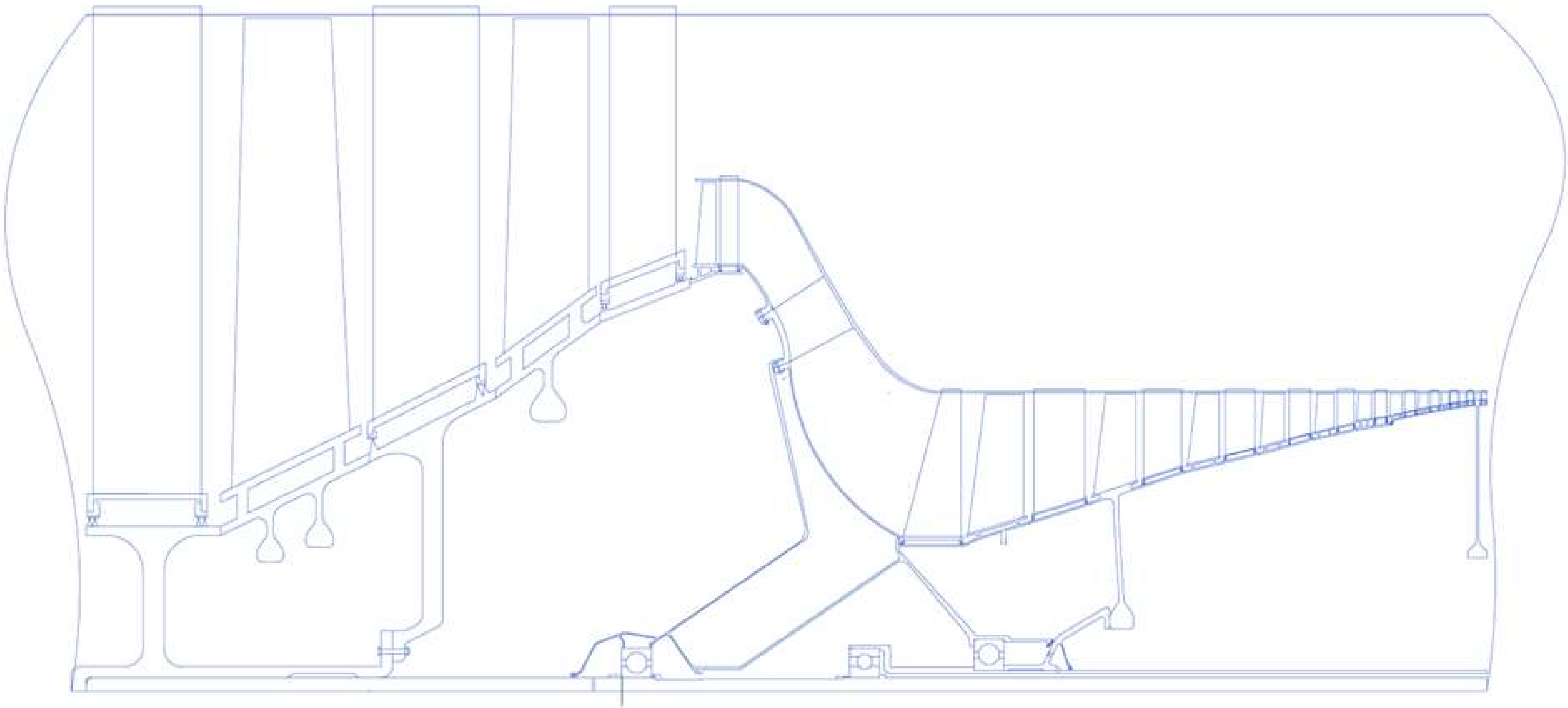

KO 22/23 Compressors Module

5.0 Combustion system

In this section all detailed information about the combustion chamber and the integrated features will be shown. KO-22/23 uses an annular combustor chamber provided with a dump diffuser and additional fuel nozzle to pre-mix the air-fuel flow. Mentioned in section 2, trade studies led our team to set T4=3197°R and Pt4=417,38 psia. Moreover, low-emission and high efficiency design is preferred.

5.1 Combustor Inlet Analysis

Airflow exits the KO-22/23 compressor with Mach Number 0.39. Velocity inside the combustor liner has to be 4-5 times lower[5.6]. At the end of the compressor a short with constant area section is applied. It minimizes the appearance of aerodynamic wakes leaving compressor exit-nozzle. The next section is a faired diffuser. The optimal opening angle (with minimal pressure losses) is between 7° and 12°[5.6]. In this section, airflow velocity is decreased to 60% of the primal value and then it is dumped to the chamber with the high cross-section area. Such a solution allows us to obtain the correct Mach Number inside the combustor liner as well as significantly lower the length and mass of the whole chamber[5.6].

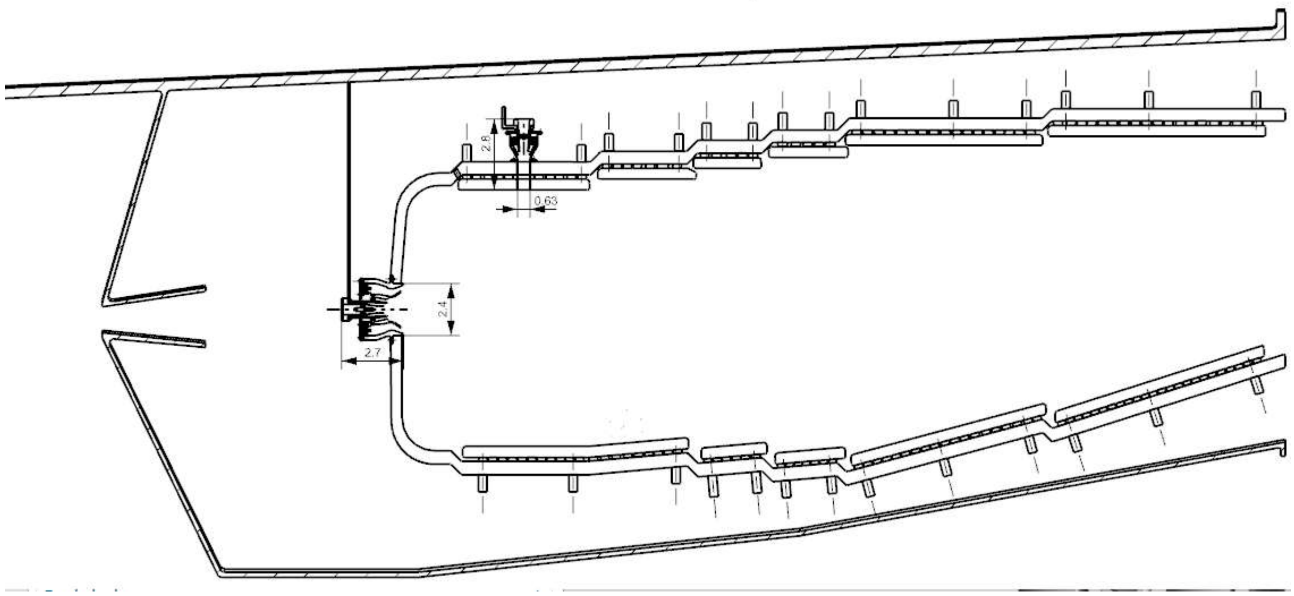

Figure 5.1 Schematic drawing of all pre-liner sections integrity

5.2 Combustor flows analysis

Airflow leaving the dump diffuser is partitioned into 4 sub-flows: Primary Zone (PZ), Secondary Zone (SZ), Dilution Zone (DZ), Cooling Airflows (CA).

Division of Mass Flow between zones is shown along with cooling effectiveness are shown in Table 5.1

$\dot{m}_{pz}$ [lb/s]	$\dot{m}_{sz}$ [lb/s]	$\dot{m}_{dz}$ [lb/s]	$\dot{m}_{ca}$ [lb/s]	$\dot{m}_{fuel}$ [lb/s]	φ_c
10.644	0	335.3	70.856	8.87	0.82

Table 5.1 Mass flow in each zone, Fuel Mass Flow, Cooling Effectiveness

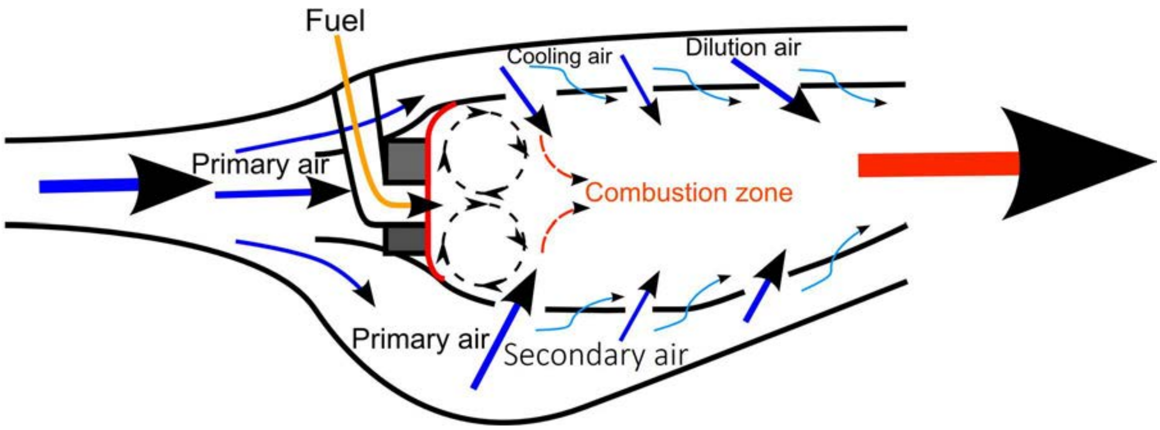

Figure 5.2 Combustor flowpath cross-section

One of the innovative solutions is Mass Flow of 0 in the Secondary Zone. This purposeful action leads to decreasing as much Temperature as possible in single row of dilution holes. This leads to significant reduction of NOx and CO due to shorter time in higher temperatures [5.5].

5.3 Combustor efficiencies

The KO-22/23 combustor has a transpiration cooling applied. From the design on cooling, the authors have taken up almost 71 lb/s of air which is nearly 17 % of the total mass flow of primary flow.

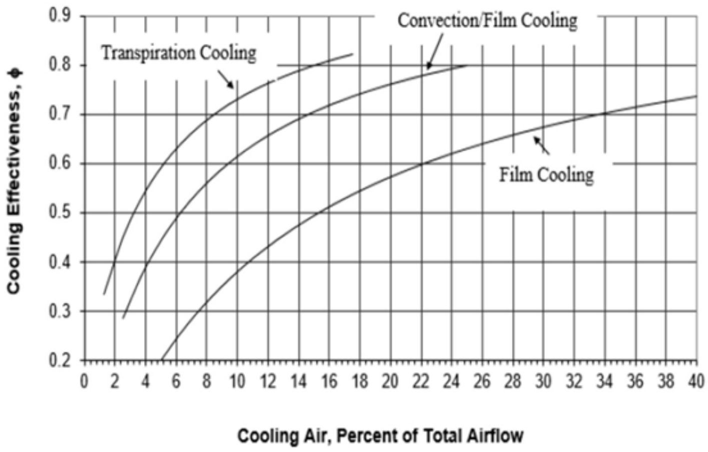

Figure 5.3 Cooling effectives in function of cooling air

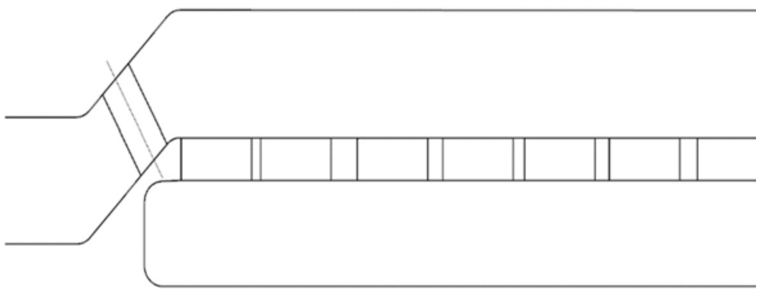

Figure 5.4 Transpiration Cooling solution applied in KO-22/23

According to Figure 5.3 KO-22/23 combustor cooling effectiveness is of 83%. Combustion efficiency is the most important parameter that describes its quality. To meet EPA requirements, the efficiency has to be at 99%. All calculation was done using Methods in Aircraft Propulsion by Farokhi.

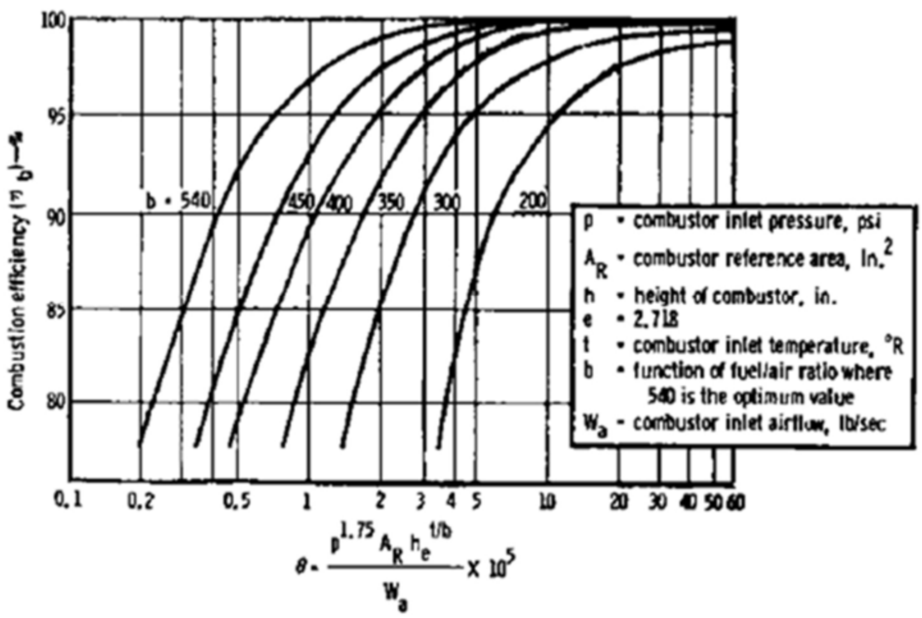

Figure 5.5 Combustion efficiency in function of CLP

Using the reaction rate parameter, b, we managed to plot Lefebvre combustor loading parameter (CLP)

b= $382*(\sqrt{2} \pm ln\frac{\varphi}{1.03}$ =453.13 (+ for $\varphi > 1.03$, - for $\varphi < 1.03$)

CLP=θ=$\frac{p3^{1.75}*Aref*h*e^{\frac{T3}{300}}}{\dot{m}t}$≈$8.09*10^5$

This results in combination with figure 5.4 gives information of nearly 100% combustion efficiency, which is satisfying to the authors.

5.4 Temperature profile

Spikes in temperature are very dangerous for combustor chambers and turbines, especially in the first stage. Therefore, the authors decided to set down the temperature profile. Based on the methodology of Farokhi, a pattern factor (PF) of 0.2 was selected, as well as a profile factor (Pf) of 1.04.

PF=$\frac{T_{tmax}-T_{tavg}}{T_{tavg}-T_{tin}}$

Pf=$\frac{T_{tmax-avg}-T_{tin}}{T_{tavg}-T_{tin}}$

Assumed PF and Pf lead to T_{tmax}=3453°R and $T_{Tmax-avg}$=3263°R

5.5 Material application

Following in the footsteps of General Electric, the authors decided to apply ceramic matrix composites (CMC) as the material for the combustor liner. CMC properties remain unchanged to temperatures of nearly 2800 °R. Mentioned in section 5.2, 17%-utilization of total mass flow as cooling airflows and applying extra protection using silicon carbide CMC's provides satisfying safety. Due to CMC application, significant length and weight saves appear as well[5.1].

According to NASA/TM—2002-211509 this material has over 260 hours of promising tests[5.2].

5.6. Combustor chamber geometry

All main geometry features will be precisely described on 2D drawings.

5.7 NOx and CO Emission

Since air traffic increased, pressure from ecologists has intensified over the years. Thus, CO and NOx emission reduction is very important. The first step into this issue the authors made by limitation of Combustor Liner Exit Temperature.

Figure 5.5 shows temperature boundaries for low emission combustion. The KO-22/23 with T4 of 3197°R (1776K) minimizes both CO and NOx emission[5.3].

NOx exact computations were done based on equations given in RFP.

$$Emission\ Mass\ per\ unit\ of\ Thrust\left(\frac{g}{kN}\right) = \sum(Emission\ index\ (\frac{g}{kgfuel}) * TSFC(\frac{kgfuel}{hr*kN}) * Time\ in\ Mode\ (hr)) = 71.8\frac{g}{kN}$$

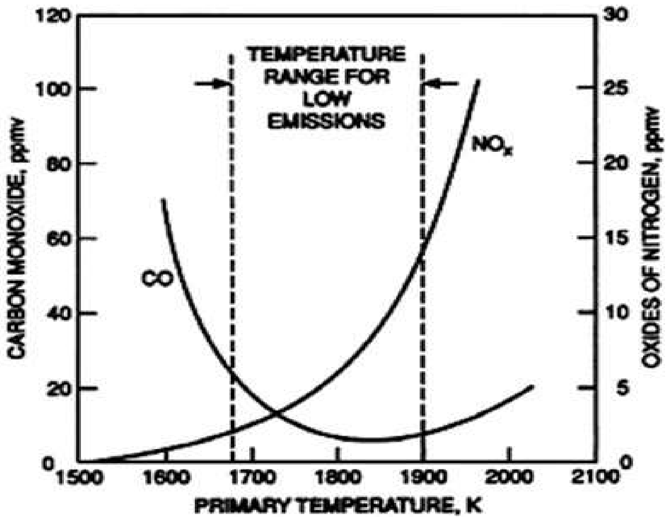

Figure 5.6 Co and NOx emission in function of temperature

$$Emission\ Mass\ per\ unit\ of\ Thrust\left(\frac{g}{kN}\right) = 36.0 + 2.42 * (OPR) = 118.1\frac{g}{kN}$$

Above total emission of NOx is given. Authors receive that result with assumption that supersonic cruise lasts for 3.5 hour. This, in turn, was assumed based on TSFC, Thrust and total fuel in a tank. [1.1]. KO-22/23 provides nearly 40% reduction of NOx compared to allowable value.

5.8 Fuel Injection

Fuel injectors are a very important factor in NOx and CO emissivity, as well as in combustion effectiveness. Carefully selecting and designing leads to success. In KO-22/23 an additional, besides the pilot fuel injector, Emission Control Fuel Nozzle (ECF), as a starter injector, and Lean Staged Fuel Nozzle (LSF), as main fuel injector, are applied. According to Japan Aerospace Exploration Agency (JAXA) this solution reduces NOx emission for 82% compared to ICAO CAEP/4 and drastic CO emission reduction. ECF with geometry is shown in Figure 5.6. It has three swirlers. The swirler vane angles are small to prevent the formation of a recirculation flow in the mixing-zone of the fuel nozzle[5.4]. The fuel is injected at a higher stream, compared to the pilot fuel injector. The modification has an effect, which makes the fuel film more uniform along with the air-fuel mixture. The airflow from the outer swirler keeps the fuel away from the fuel nozzle wall[5.4].

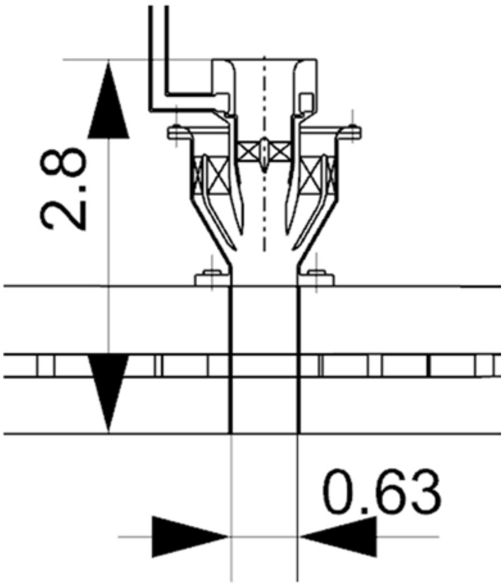

Figure 5.7 LSF Scheme with geometry properties.

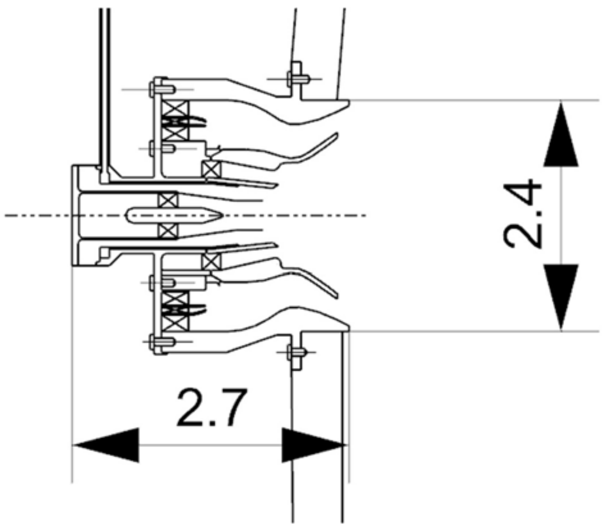

Figure 5.8 ECF Scheme with geometry properties

6. Turbine design

Introduction:

This engine contains a high pressure (HPT) and Low Pressure (LPT) Turbine, The first supplies Power to the HPC and the LPT provides Power to the fan and LPC. Everything works In two spool-system. This part of report includes: cycle analysis, material , blade and disk design, bearings, cooling.

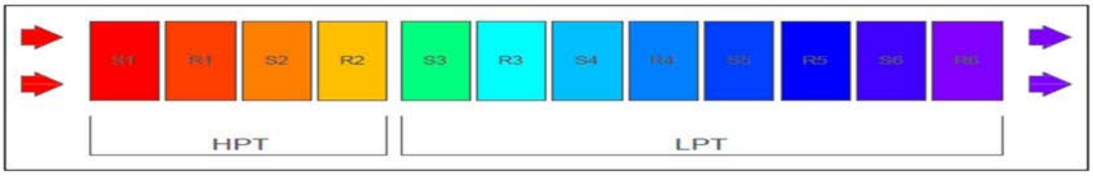

Figure 6.1 Scheme of KO 22/23's turbine.

6.1 Flow Calculation

This part contains absolute and relative flow paths In the HPT and LPT. Turbine was design to have a constant inner radius and axial velocity. Starting with parameters showed In „Gasturb 13", a step by step process was followed to calculate the velocity triangles on each stage. [6.1]

Design parameter	Value
$\dot{m}$(lb/s)	164.64
T_1(°R)	3194
P_1(psia)	176.805
Density (lb/ft^3)	0.1486
ω_{HPT} (RPM)	9850
ω_{LPT} (RPM)	4230

Table 6.1 Inlet Pitchline flow parameters are taken from Gasturb 13 for the turbine of KO 22/23 at fly.

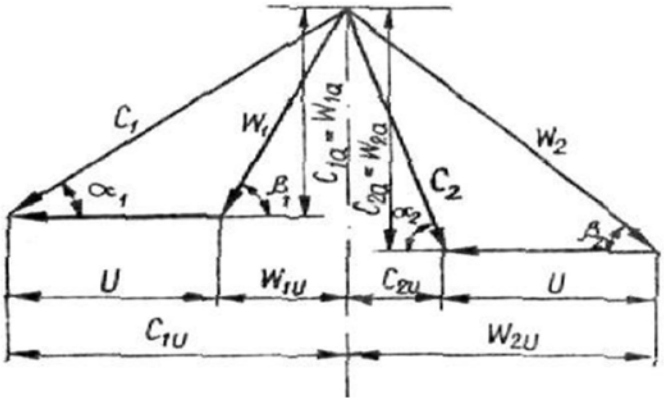

Figure 6.2 General scheme of turbine's velocity triangles and angles. [6.2]

	C(ft/s) absolute velocity			W(ft/s) relative Velocity			U(ft/s) rotation velocity			Mach number absolute/relative		
	Hub	Pitchline	Tip	Hub	Pitchline	Tip	Hub	Pitchline	Tip	Hub	Pitchline	Tip
Nozzle1	1958.20	2070.76	2183.59	1198.65	1217.81	1237.00	-	-	-	0.77/0.47	0.82/0.48	0.86/0.49
Rotor1	1530.11	1543.93	1554.85	1758.72	1823.75	1890.02	791.47	886.18	980.9	0.70/0.61	0.73/0.62	0.77/0.63
N2	2043.7	2162.50	2281.66	1284.21	1307.9	1331.66	-	-	-	0.86/0.55	0.90/0.58	0.92/0.60
R2	1751.11	1891.79	2020.31	1954.00	2127.19	2290.05	791.47	887.86	984.25	0.85/0.76	0.89/0.91	0.94/0.98
N3	886.15	938.35	990.81	573.26	584.05	594.91	-	-	-	0.38/0.25	0.42/0.26	0.45/0.27
R3	808.07	823.88	886.07	889.73	924.24	998.22	339.89	382.38	424.86	0.35/0.39	0.37/0.41	0.40/0.45
N4	927.75	1006.95	1088.12	623.12	659.41	683.95	-	-	-	0.41/0.28	0.46/0.30	0.50/0.32
R4	828.31	895.70	951.73	908.13	995.83	1074.17	339.89	397.27	454.62	0.37/0.40	0.41/0.45	0.44/0.50
N5	958.85	1032.18	1142.84	665.68	675.85	710.13	-	-	-	0.42/0.28	0.46/0.29	0.53/0.32
R5	900.16	952.19	1035.20	974.14	1053.80	1163.28	339.89	412.14	484.41	0.37/0.41	0.45/0.50	0.47/0.54
N6	973.45	1090.97	1220.96	672.44	705.18	748.26	-	-	-	0.45/0.31	0.52/0.34	0.60/0.37
R6	869.94	981.46	1164.33	946.88	1087.27	1293.43	339.89	427.03	514.20	0.40/0.44	0.47/0.52	0.58/0.64

Table 6.2 Detailed velocities on each stage (red colour - parameters of HPT, LPT-yellow colour)

	α(deg)			β(deg)			Degree of reaction		
	Hub	Pitchline	Tip	Hub	Pitchline	Tip	Hub	Pitchline	Tip
Nozzle1 α_1 / β_1	12.67	11.97	11.34	21.00	20.65	20.32	-	-	-
Rotor1 α_2/ β_2	87.03	86.70	86.38	60.32	57.68	55.18	0.28	0.30	0.33
N2 α_1/ β_1	11.34	12.86	12.14	20.32	20.75	20.35	-	-	-
R2 α_2/ β_2	86.38	87.40	87.30	55.18	63.54	62.66	0.34	0.37	0.4
N3 α_1/ β_1	18.23	17.18	16.25	28.92	28.34	27.78	-	-	-
R3 α_2/ β_2	87.58	87.33	87.24	65.15	62.92	62.08	0.32	0.36	0.38
N4 α_1/ β_1	25.00	22.91	21.12	38.05	36.48	34.98	-	-	-
R4 α_2/ β_2	87.64	87.45	87.26	65.68	63.97	62.25	0.29	0.33	0.35
N5 α_1/ β_1	24.78	22.91	20.59	37.73	37.43	35.21	-	-	-
R5 α_2/ β_2	87.64	87.54	87.17	61.66	64.75	61.53	0.32	0.36	0.38
N6 α_1/ β_1	22.60	20.05	17.84	33.80	32.03	29.99	-	-	-
R6 α_2/ β_2	87.76	87.50	87.46	66.74	64.40	64.06	0.29	0.40	0.42

Table 6.3 Detailed angles on each stage (red colour - parameters of HPT, LPT-yellow colour)

6.2 Velocities step-by-step calculation

Here we provide handmade velocities triangles calculation for the first stage of HPT

k-isentropic coefficient
R- gas constant

Firstly we find turbine work which must be provided to HPC

$l = \frac{k*R}{k-1}(T_3 - T_2)$ =690906.2 J

Then we calculated work divide between stages:

$l_{st} = \frac{\mu_{st1}}{\sum_{i=1}^{n} \frac{\mu_{sti}}{q^{n-1}}} l$ =329003 J for the first stage

μ- load coefficient

q -divide coefficient

Then velocity c_1 on pitch line must be find.

$c_1 = \varphi\sqrt{2l_{st}(1-\rho)}$ =2070.77 ft/s

ρ- degree of reaction on pitchline

$c_{1a}=c_1\sin\alpha_1$

$c_{1u}=c_1\cos\alpha_1$

then we calculate velocity U:

$$U = \frac{\pi n D}{60} = 885.82\frac{ft}{s}$$

Then:

$$\beta_1 = atan\frac{c_{1a}}{c_{1u}-U} = 0.36rad$$

later we may count:

$$w_1 = \frac{c_{1a}}{sin\beta_1} = 1217.81\frac{ft}{s}$$

and:

$$w_2 = \delta c_1\sqrt{\frac{\rho}{1-\rho}\frac{1}{\delta_n^2} + (\frac{w_1}{c_1})^2} = 1823.75\frac{ft}{s}\delta - rotor\ speed\ coefficient$$

$\delta_n - nozzle\ speed\ coefficient$

$w_{2u} = (1+\vartheta)U = 974.80\frac{ft}{s}$

$$w_{2a} = \sqrt{w_2^2 - w_{2u}^2} = 1541.37\frac{ft}{s} C_{2u} = w_{2u} - U = 88.61\frac{ft}{s}\beta_2 = atan\frac{w_{2a}}{w_{2u}} = 1.00rad \propto_2 = atan\frac{C_{2a}}{c_{1u}} = 1.51rad$$

We have all velocities and angles on pitchline, then same way should be used to count them on other radiuses. Same way of counting was used to make LPT.

6.3 Flow parameters:

This part contains calculated distribution of parameters such as temperature and pressure on blades on each stage. [6.1]

Total temperature [°R]			
	Hub	Pitch	Tip
N1	2963.98	2936.88	2908.18
R1	2845.44	2809.86	2768.47
N2	2595.77	2530.33	2457.28
R2	2437.43	2353.80	2271.01
N3	2389.99	2301.17	2211.69
R3	2362.29	2270.35	2178.29
N4	2310.29	2209.74	2106.75
R4	2282.68	2178.65	2073.79
N5	2230.60	2118.95	1999.80
R5	2200.23	2077.50	1960.43
N6	2142.98	2006.36	1870.36
R6	2094.59	1966.04	1837.31

Table 6.4 Temperature distribution on blades on each stage (red colour - parameters of HPT, LPT-yellow colour

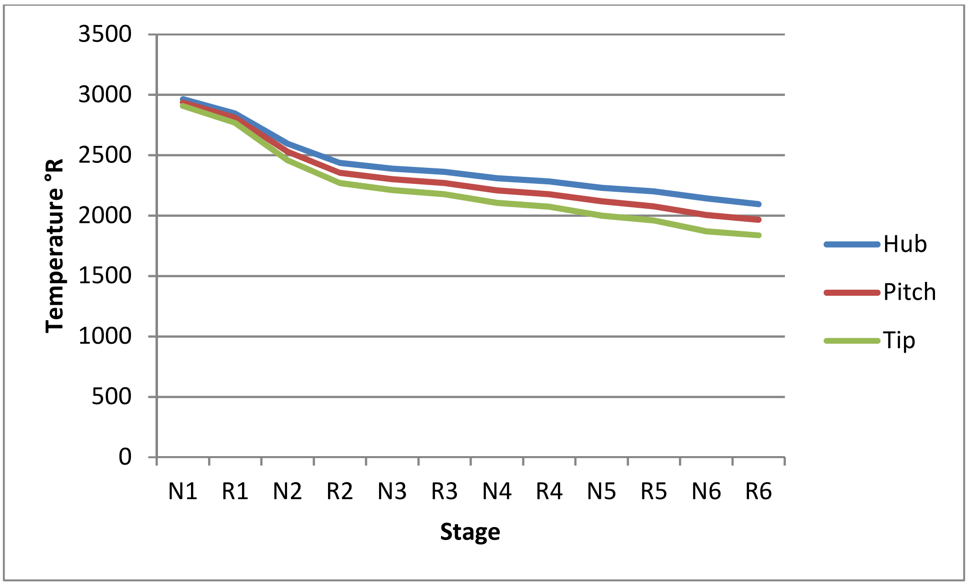

)

Figure 6.3 Temperature distribution ono blades on each stage

Total pressure [Psia]			
	Hub	Pitch	Tip
0	176.8	176.83	176.83
N1	122.32	116.89	111.36
R1	96.51	92.04	86.07
N2	61.28	54.81	48.29
R2	43.58	37.2	32.38
N3	39.57	33.33	28.52
R3	37.18	30.99	26.27
N4	33.34	27.18	22.38
R4	31.27	25.72	21.01
N5	27.92	22.47	17.65
R5	25.95	20.19	15.85
N6	22.71	17.53	13.64
R6	20.10	15.39	12.14

Table 6.5 Pressure distribution on blades on each stage (red colour - parameters of HPT, LPT-yellow colour)

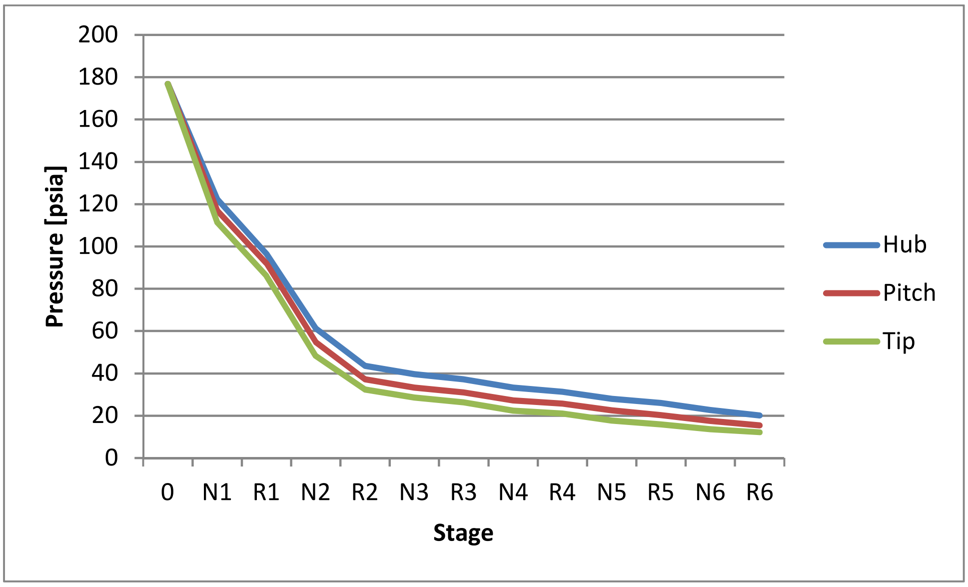

Figure 6.4 Pressure distribution on blades on each stage

6.4 Material Selection

From the beginning of aircraft there is seen a trend to maximize efficiency and performance of planes and engines but such strenuous requires modern, tough and immune to high temperatures material. Presently nickel-based super-alloys are in use, however, as engines works in higher temperatures, these alloys became inadequate and more complicated and advanced cooling systems are necessary. [6.3] That means a need of searching for a new material. And ceramic matrix composites seem to be a good candidate for a successor. These materials consist of fibbers cured in a matrix, usually carbon or silicon carbide. Silicon carbide fibres and silicon carbide matrix CMCs (SiC/SiC) are a good choice because of their thermal properties. They require not so much or even no cooling and are 60% lighter than nickel alloys [6.4] Because of those facts SiC/SiC was chosen as a material for KO 22/23's turbine. That material is also attractive since General Electric tested it in 2015 in a GE F414 turbofan engine. [6.5] „The F414 CMC test -- which endured 500 gruelling cycles – validated the unprecedented temperature and durability capabilities of turbine blades made from lightweight, heat-resistant CMCs, allowing for expansive deployment of the advanced manufacturing material in GE's adaptive cycle combat engine and next-gen commercial engines." [6.6] Also that material was tested for up to 400 hours In 2642 °F and using tension of 10 KSI showed up to 0.7% tensile strain.[6.7]

Material property:	Value
Young modulus [Msi]	43
Max service temperature [°R]	3.37

Table 6.6 Material Properties of SiC/SiC Ceramic Matrix Composite [6.8]

6.5 Cooling system

One of the consequences of high temperatures on first stages of turbine is need of using cooling system. Although as it was said previously SiC/SiC CMC has great thermal properties, however, there occur local temperature strikes up to 3440 °R (look combustor section) and even this material can't resist such tensile. Because of that fact there would be used thermal barrier coating Al2O3–Y2O3 which would increase thermal resistance for about 200 °R [6.9]. Moreover, due to the fact that KO-22/23 would be used in airliner and high durability of parts is one of main points lead to conclusion to use a film cooling on first stage of turbine.

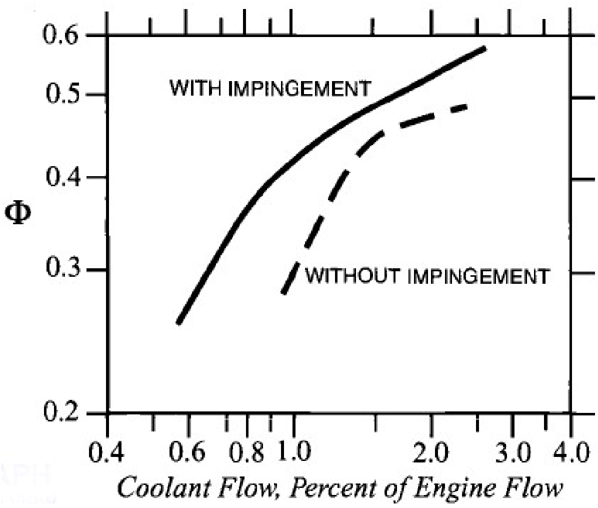

Figure 6.5 Coolant Flow, Percent of Engine Flow

Cooling air value of 2% on rotor and 2% on nozzle seems adequate. As seen in figure 6.3 [6.10] 2% coolant flow responds around 0.55 cooling effectiveness. Cooling air would be taken from the last stage of HPC and would have around 1620° R which will reduce temperature on the first nozzle of HPT to ≈2610°R [6.1] and it is surly enough to increase its life time.

6.6 Turbine blade design and stress consideration

Blade design has been done using Farokhi, S, "Aircraft Propulsion." Turbine was designed due to constant inner radius, also Zweifel coefficient was assumed as 1.

Stage:	N1	R1	N2	R2	N3	R3	N4	R4	N5	R5	N6	R6
HUB Radius [in]	18.42	18.42	18.42	18.42	18.42	18.42	18.42	18.42	18.42	18.42	18.42	18.42
Pitchline [in]	20.62	20.62	20.66	20.66	20.71	20.75	21.49	21.52	22.32	22.36	23.11	23.14
Tip [in]	22.83	22.90	22.91	22.94	22.95	23.00	24.56	25.1	26.22	26.25	27.87	27.91
Area [in^2]	61.06	63.02	63.30	64.15	64.43	65.86	117.37	118.80	190.11	192.65	280.40	282.78
AN^2*10^9 [in^3/s]	5,92	6.11	6.14	6.22	1.14	1.17	2.09	2.11	3.40	3.43	5.00	5.04
σ_c[psi]	260961	269337	270620	274039	48114	49160	87625	88745	141998	143492	209218	210712
Blades number	121	121	119	119	119	119	111	107	99	97	83	81
Chord [in]	1.47	1.49	1.50	1.50	1.51	1.52	2.04	2.22	2.60	2.61	3.15	3.16
Blade spacing [in]	0.86	0.86	0.87	0.87	0.89	0.89	0.94	0.95	0.97	0.97	1.01	1.01

Table 6.7 Blade design and stress parameters (red colour - parameters of HPT, LPT-yellow colour)

Since radius of flow path is almost not changing on HPT that number of blades is same, important changes became from the stage four. Also because of some tip clearance and some bleedings it is advised to use labyrinth casing. It would decreases significantly flow loses on stators, moreover casing would be integrated in rotating blade rows.

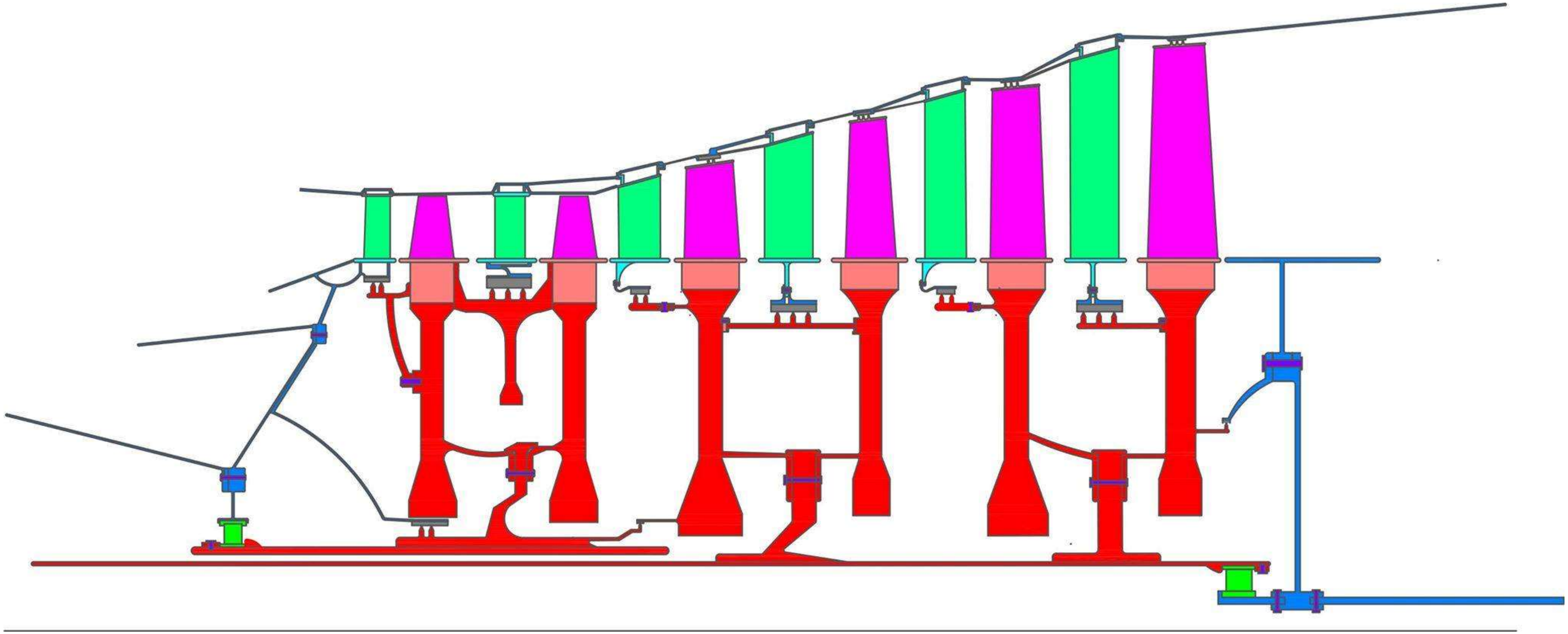

Figure 6.6 Detailed scheme of turbine

7. Nozzle

7.1 Main design

The propulsion system of supersonic engine needs nozzle with great performance. In fact, a I-percent gain here is at least three times as effective as a I-percent gain in performance of any other component. A I-percent change in subsonic cruise thrust coefficient affects range by about 2 percent, and the sensitivity to loiter thrust is the same as it was before. It can be worth a great deal of nozzle weight to keep performance high at all flight speeds[7.2]. Next generation engines require multi-dyscypline trade-off study. The exhaust nozzle system for a supersonic cruise aircraft mandates additional features such as variable throat and exit area, jet noise suppression, and reverse thrust. Main target is to reduce noise. To start with jet velocity which has great influence on jet noise as well on take off thrust. The solution turns out as an axillary inlet-ejector, [7.11]The velocity of exhaust gases will be reduced from 1450ft/s to about 1250ft/s.[]

It was turned out that the variable geometry of convergent-disconvergent nozzle meets great efficient at all conditions. Despite of complication of construction and increased mass choose an C-D nozzle is a reasonable. There are three type general types of variable geometry nozzle as variable A8 or variable A9 or both. Control system of nozzle geometry is provided by movable flaps in 8 section and movable C-D flaps, on the one hand it is dedicated by ejector implementation, on the other it may turn out efficiency, figure[7.1].

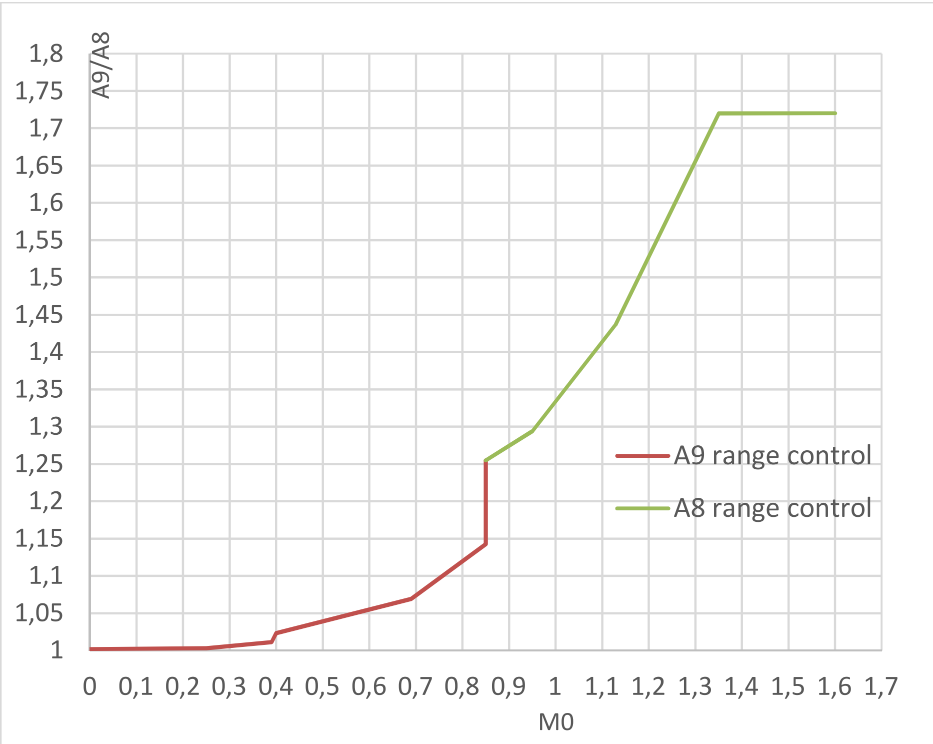

Figure 7.1 Nozzle area ratio schedule

Auxiliary-inlet ejector nozzles have been used on the F-l11 and SR-71 aircraft and are being considered for low-noise nozzles. The ejector flow model is based on the inviscid and viscid interaction between a high-energy stream (primary flow) and a low-energy stream (secondary flow) as shown in Figure 7.2. These two streams begin to interact at the primary nozzle lip. For the ejector operating in the supersonic regime the secondary flow is effectively "sealed off" from ambient conditions. When this occurs, the ejector mass flow characteristics become independent of the ambient static pressure. It is this ejector operating condition that is considered in the theoretical analysis. The flow regimes occurring within the ejector system can be categorized on the basis of the predominant flow mechanisms. When the secondary flow to the ejector is low , the primary flow plumes out and impinges on the shroud wall. This causes an oblique shock to form and effectively seals off the secondary flow from ambient conditions.

The secondary flow is " dragged" through the oblique shock by mixing with the higher velocity primary jet flow. If the secondary flow is increased, the secondary pressure increases and pushes the primary jet away from the shroud wall. Because the oblique shock can no longer be sustained at the shroud wall , the secondary flow accelerates and chokes within the shroud.

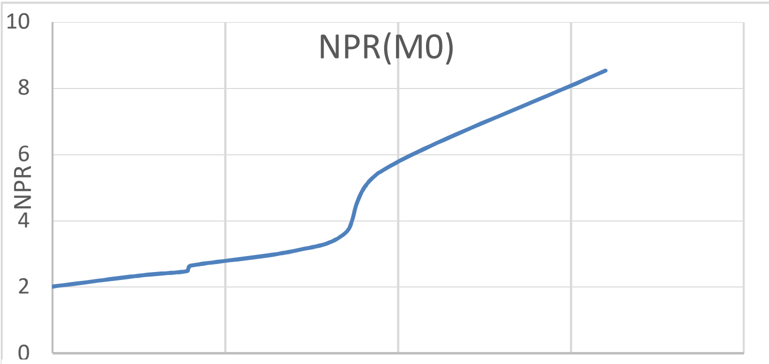

Figure 7.2 NPR schedule

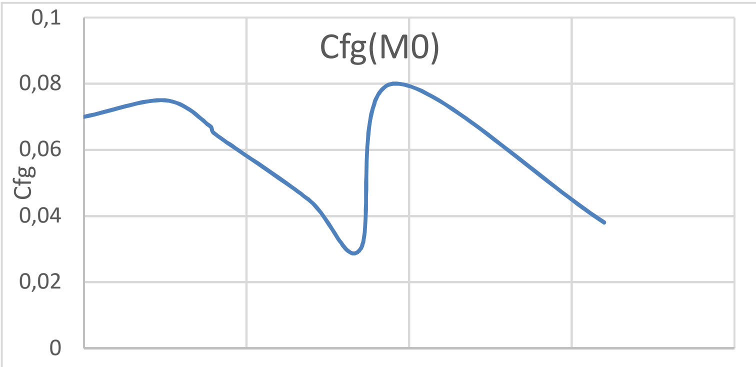

Figure 7.3 Gross thrust coefficient schedule

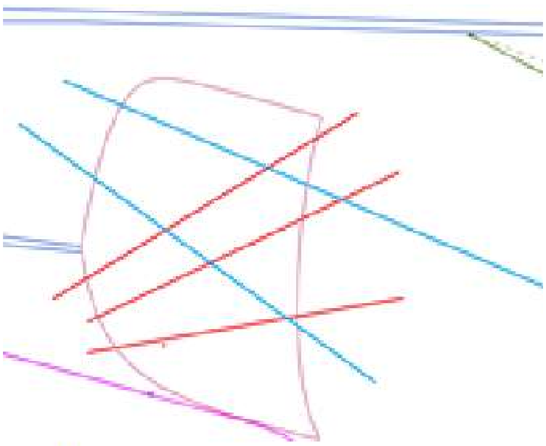

a) Low secondary flow

The first step in calculating the performance of an exhaust system for a supersonic cruise aircraft is to get some idea how sensitive a mission is to its design. Some results of an analysis Getting enough range out of a supersonic cruise aircraft has always been a fundamental problem, and it is even more critical for commercial operations. For this mission the cruise nozzle efficiency affects range by 3.5 percent and is quite important. In fact, a I-percent gain here is at least three times as effective as a I-percent gain in performance of any other component of the propulsion system A I-percent change in subsonic cruise thrust coefficient affects range by about 2 percent, and the sensitivity to loiter thrust is the same as it was before. It can be worth a great deal of nozzle weight to keep performance high at all flight speeds.[7.2]

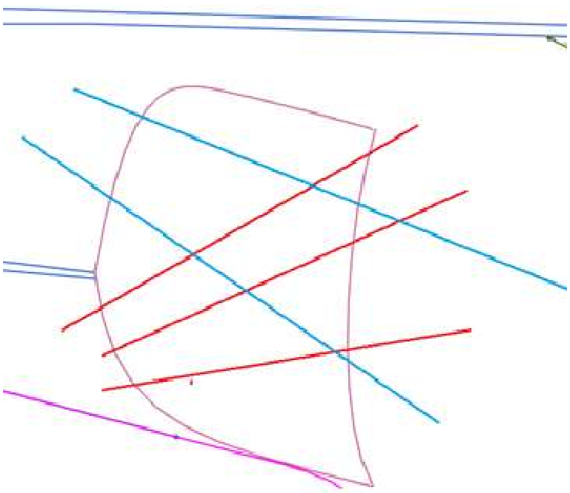

b) Hight secondary flow(choke)

The General Electric Company estimated that a 1-percentage-point change in transonic acceleration gross thrust coefficient is equivalent to a 2000-lb change in takeoff gross weight for a typical supersonic cruise aircraft. The sensitivity is therefore about one-fifth of that at supersonic cruise. The SCR program did not set a study goal for this flight condition, but a nozzle efficiency of 0.95 would probably be realistic 1% change in subsonic nozzle gross thrust coefficient is equivalent to a 3000-lb change in TGW for a typical supersonic cruise aircraft with a range of 4000 n mi and a 600-n mi subsonic cruise segment. This sensitivity is about one-third that at the supersonic cruise condition. The fight is for the every percent of gross thrust coefficient on cruise. A I-percentage-point change in nozzle gross thrust coefficient at takeoff was equivalent to only 750 lb in takeoff gross weight, in contrast to 10 000 lb at supersonic cruise and 3000 lb at subsonic cruise.[7.2]

7.2 Axillar Ejector

The door of ejector are consist of two convergent beams, movable convergent-disconvergent flaps with has aerodynamic shape which has low drag factor, and may easily fit in nacelle during cruise. Moreover it has 15deg. boattail angle, analised as most effective. TSFC probably increase a little, but thrust should stay the same. The control system is provided by 4 servomotors and connected oil installation with A_8 control mechanism.

The ejector inlet doors serve two main functions within the exhaust nozzle. They provide for the opening and closing of the ejector inlets and form a portion of the subsequent flowpath for the external free-stream air and the engine flow. Therefor it improves regulation of A_9/A_8. In 25% control of nozzle geometry provide movable flaps on the end off nozzle(variable A_9). Moreover “cold” air may be used for the same purpose, then feed in 8 section decrease, but it needs wider analysis, figure 7.5. This variation unfortunately is connected with inlet doors through air is supplied. During subsonic and supersonic cruise control of nozzle geometry is enabled by movable A_8.

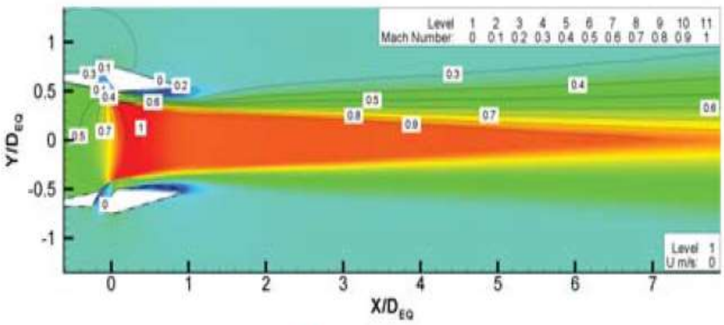

(e) Rolls-Royce HYDRA-CFD prediction

Figure 7.11 Nozzle velocity[7.3]

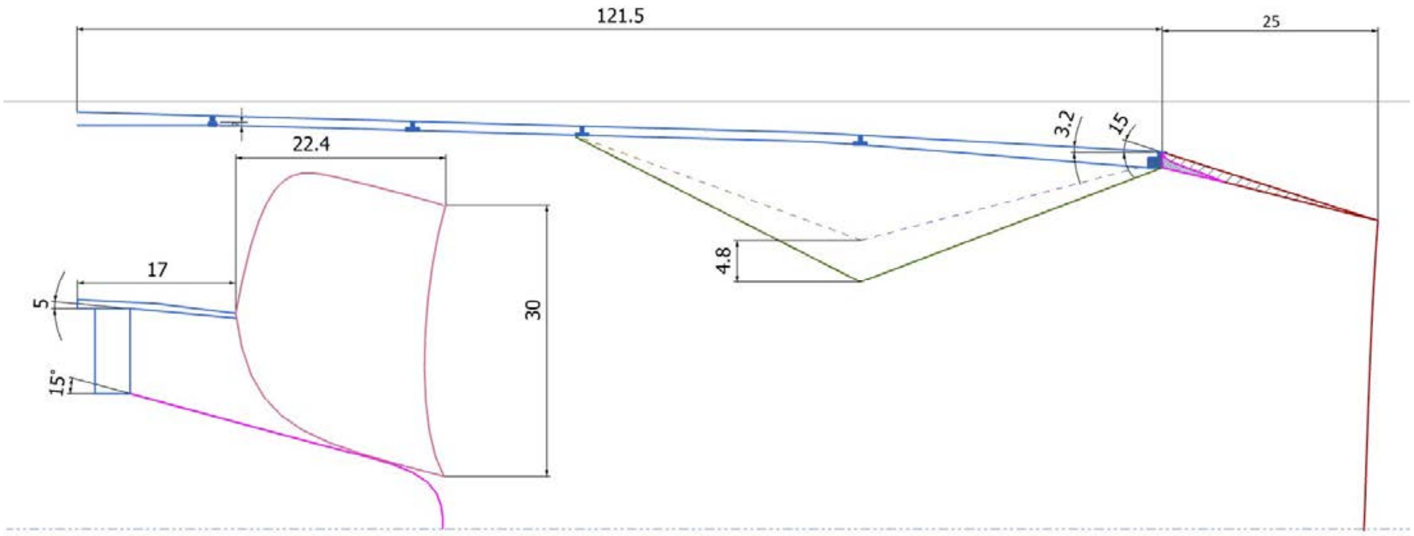

Figure 7.5 Schame of KO-22/23’ nozzle system- dotted line symbolize variation of A8 area

This kind of nozzle design may cause choke of nozzle. But in this studies it is predicted and variable of A_8 is slightly (radial feed of servomotor is 5in.).

Chevrons The application of chevrons on the ejector nozzle is expected to result in the enhanced spreading of the jet and forces the shear layer to attach to the inner surface of the clamshells thereby reducing the flow separation. In addition to the ejector nozzle performance improvement, chevrons have noise suppression capability in the low frequency part of the spectrum [7.3]. Large amplitude screech tone reduction were identified as a direction result of the drastic cross sectional modification, with reduction in the 7-8dB range achieved at all operation conditions[7.8].

7.3 Mixer

The fan/core mixer design was to serve multiple purposes. It was located just aft of the turbine exhaust case (Figure 7.8), and the basic functions were to:

1. Mix fan and core flows to reduce gas temperature, extending mixer/ejector life
2. Hold fan pressure ratio constant to operate at high efficiency
3. Increase stall margin
4. Improve specific fuel consumption
5. Suppress noise through improved hot/cold-stream mixing

Aside from performance, a fixed-area fan/core mixer would be much easier to design, due to the removal of moving parts, and offer the added benefit of weight reduction. performance losses. There was a small performance loss at subsonic cruise (about 3%) at 60% thrust setting. Takeoff performance differences between variable and fixed mixers were negligible. The design effort at that point was redirected to develop the fan/core mixer as a fixed-area concept (Figure 7.5). To provide mixer lightweight while making it strong enough to overcome the vibration characteristic of a large-panel .
Design Issues – The prominent design challenge to a fixed-area fan/core mixer is to keep the mixer lightweight while making it strong enough to overcome the vibratory characteristics of a large-panel Structural – In the context of viewing the nozzle as a long axial box neccel which is the principal structural members of the nozzle. Sidewall is interrupted by axillar door inlet. These sidewalls are 2.5 in thick and constructed of 6-2-4-2 Titanium truss core. The integral beams are formed 6–2–4–2 Ti sheet metal with a typical thickness ranging from 0.045 to 0.063 in. Analysis indicated that, with a good fan/core mixer, improving flow coming into the mixer and improved ejector acoustic lining could reduce this penalty to 0.5 EPNdB or less.[7.1]

Figure 7.12 Front look of KO-22/23' mixer

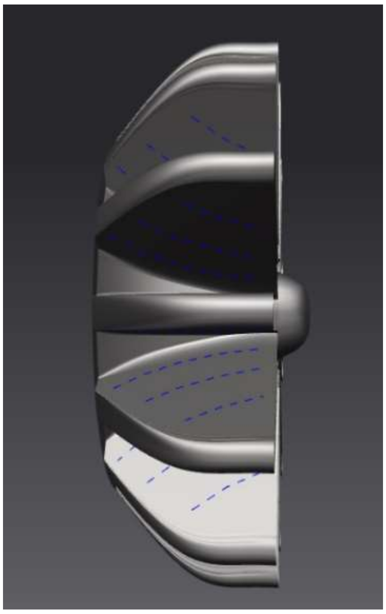

Figure 7.13 Right look of mixer. Blue lines symbolize score guides

Mixer efficiency is estimated for 85% with all responsibility, and no losses through mixer[7.1] (underestimated 0.98 in GasTurb calculations). It is justified by the trend, in the 1960-s this factor was estimated for 0.85, and 0.67 was achieved[7.5], but in 2005 during NASA calculations it was 80%.[7.1]

Acoustic Tiles

An enabling, ceramic-matrix-composite, acoustic-tile design could allow the HSCT to use a higher temperature capability and/or lighter acoustic liner relative to the baseline CPC metallic liner. The acoustic tile was designed specifically for noise suppression. It was considered two distinct methods of using tiles for noise suppression. The first was a SDOF sandwich structure consisting of two face sheets with a honeycomb core. The top, cold sheet is solid, but the bottom sheet is perforated. The porosity is on the order of 10 to 12% (Figure 7.6).This style of suppression is tuned to reduce a specific frequency. Although it does a good job for a specific frequency and is a proven design, it offers little suppression for other frequencies. In addition, this design is conventional for metallic liners; however, it is very difficult to fabricate from CMC. The broad-band design offers much more benefit in terms of design and fabrication flexibility. It is easier to design with because it allows suppression for a wide range of frequencies as well as allowing more room for error when defining the specific frequency band of interest. This design consists mainly of a single, high-porosity face sheet with a porous foam absorber backing. This particular design also has a thermal-protection system that does not assist in noise suppression but protects the back structure from hot exhaust gas. This design varies significantly from typical 2D nozzles that have cooled liners. The acoustic liners allow hot exhaust gas to pulse in and out through the holes in the porous face sheet in order to suppress noise. This air infiltrates the porous foam and comes into contact with the back structure.[7.1] This broad-band design is relatively simple; therefore, fabrication options are tiles are the baseline design for the KO-22/23 nozzle. They are located primarily on the nozzle divergent flaps and aft of the mixer[7.1].

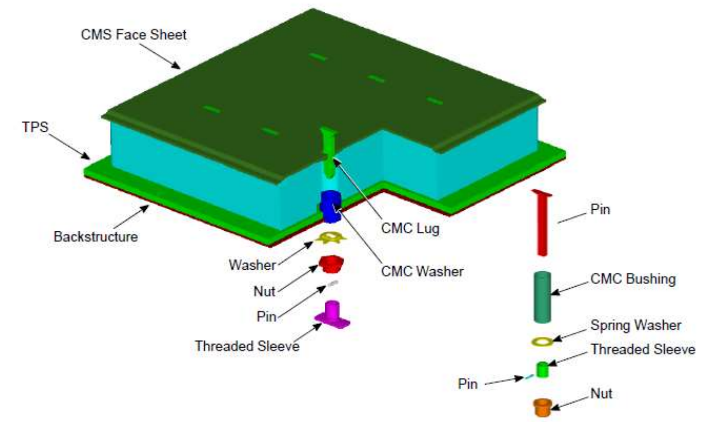

Table 1 Figure 7.8 Acoustic tile strucyure [7.1]

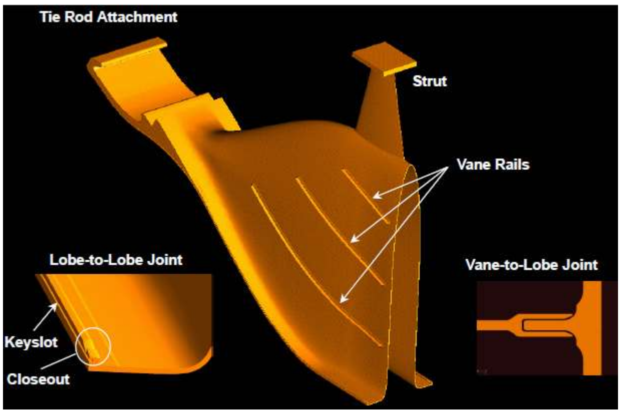

Figure 7.914 Mixer structure[7.1]

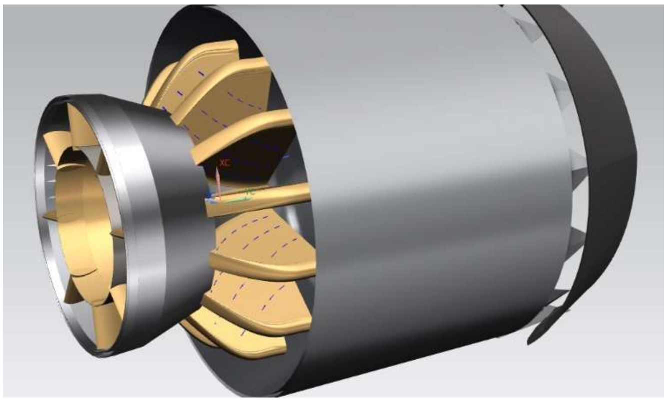

Figure 7.10 View of mixer and nozzle

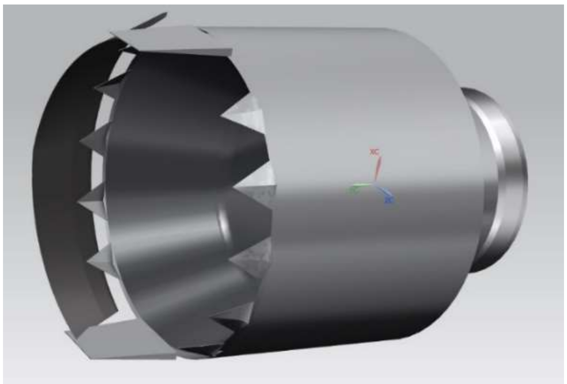

Figure 7.11 Integrated chevrons

Materials

Centerbody(plug)-CMC; Mixer-TiAl, midframe-Inco 718, Divergent flaps-TiAl, Ejector doors-Inco 718, Sidewalls-TiAl, Chevrons-Inco 718, Duct-Inco 718,

Noise

The maximum noise levels of those aeroplanes covered by, when determined in accordance with the noise evaluation method of Appendix 1, shall not exceed the following: 108 EPNdB for airplanes with MTOW 272 000kg, and 102EPNdB at 34 000kg. It is require to achieve, for 130 000kg airplane, approximately 106EPNdB, and 100EPNdB at flyover[7.6]

Estimation of noise reduction of KO-22/23

-exhaust velocity V_9~1250ft/s (ideal would be 1100ft/s, what might be achievable in case of increasing axillar inlet flow)

-chevrons-12 of them installed in inlet door, noise amplitude reduction of 7-8dB and screech 10-25dB[7.8]

-long duct forced mixer-1-2EPNdB at Lateral and takeoff; TRL 6-7[7.7]

-acoustic tiles-suppression mixing low frequency noise[7.1]

-inlet liners, and liners integrated with anti-icing system; TRL 4-6; 1-3dB[7.7]

-zero splice inlet liners; TRL 7-9; 1-4dB[7.7]

-turbine-hot stream acoustic liners, aerofoil counts; TRL 9; 2-4dB reduction[7.7]

-combustor-cavity acoustic plugs; TRL 4-5; 4-9dB[7.7]

-3 to 4 dB in broadband noise may be achieved by aerodynamic and geometric blade
optimization via swept rotor design and swept and/or leaned stator designs, active stator 5-8dB (TRL 3)[7.7]

8. Bearings

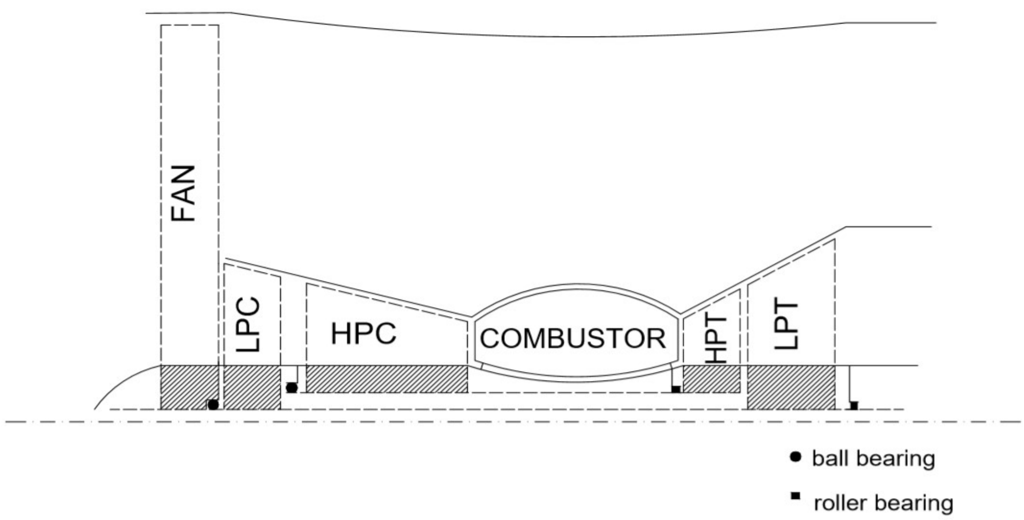

Figure 8 .1 Scheme of engine and places of bearings

Even the best rotating machinery especially jet engines to work efficiently and to be stable needs well placed and high quality bearings. As a main design option was decided to use classical bearings , which are well-know and reliable, as ball and roller bearings. These are cheap and technology of usage and production are mastered. For this bearings would be used metal named: M50NIL. It is a high speed bearing steel that is melted as VIM + VAR melt type. This grade has increased molybdenum which helps improve wear resistance and strength at high temperatures. [8.1]

Also as an alternative was predicted usage of foil bearings. These bearings were designed specifically for high speed and high temperature applications and were successfully tested on Boeing 737 during the early 1960s. Drawback of it is complicated system of air delivering and need of taking some part of air mass flow from the compressor which obviously will reduce such parameters like thrust.

9. The lubrication system

The lubrication system which we use is dual cycle installation. It is built similar to installation working in a shortened cycle, but around 10% of the oil from the cooler is directed through the reactor to the tanks. So in this kind of installation 90% of oil circulates skipping the oil tanks, but the remaining part does flow through. Behind it, a pump id placed which gives oil to the force pump. The diagram of the dual cycle installation is shown in figure 9.1. [9.1]

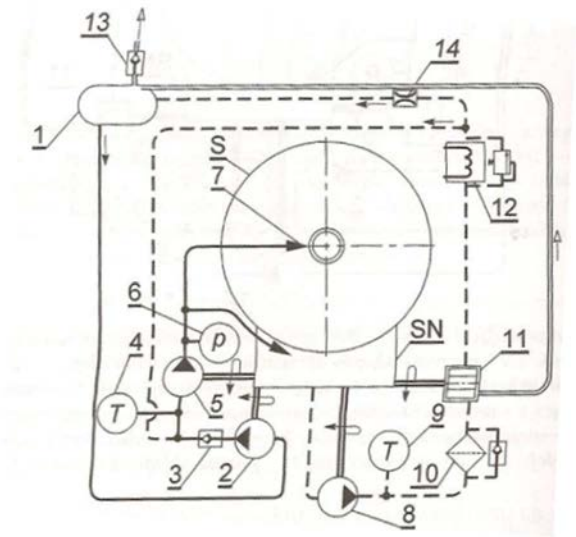

Figure 9.1 Diagram of the dual cycle installation. 1- oil tanks, 2- auxiliary pump, 3- check valve, 4- heat sensor of forced oil, 5- force pump, 6- pressure sensor, 7- oil injector, 8- suction pump, 9- heat sensor of oil extracted from the engine, 10- filter, 11- centrifugal froth breaker, 12- cooler of the oil, 13- reduction valve, 14- reactor [9.1]

10. The fuel system

The fuel system works closely with the engine management system but also with auxiliary installations, for example oiling. Applied by us the fuel system was used by jet engine CFM-56 which was flying in an airliner Boeing B737. The fuel from tanks flowing through the filters is directed to set of engine fuel pumps. The fuel is served first to the low-pressure pump, therefore subsequent flowing to the fuel-oil heat exchanger of electric generator and oil installation, then to the high-pressure pump. From this pump the fuel flows to the hydromechanical regulator, then through the electrohydraulic pilot valve that measures amount of fuel flowing. From the hydromechanical regulator, the fuel that flowed through a flow meter is directed to the combustion chamber injector. Excess fuel delivered to the electrohydraulic pilot valve is directed back before the high-pressure pump. Part of the fuel pressed through high-pressure pump is used as a hydraulic fluid. This fuel is delivered from the hydromechanical regulator to the actuators, enabling the adjustment of variable stator blades. The power supply system also comes through the airframe and engine stop valves, which ensure the safe operation of the engine and fuel cleaning filters. [10.1]

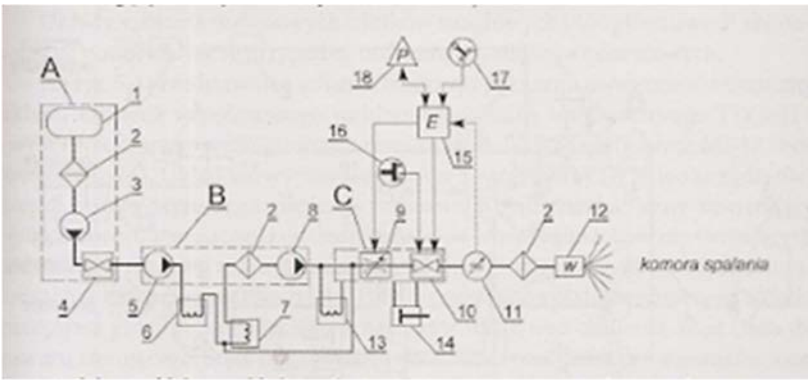

Figure 10.1 Flow chart of fuel supply system: A-airframe, B-pump set, C-hydromechanical regulator; 1-fuel tanks, 2-filters, 3-pump, 4-engine stop valves, 5- low-pressure pump, 6- fuel-oil heat exchanger of electric generator, 7- fuel-oil heat exchanger of oil installation, 8-high-pressure pump, 9- electrohydraulic pilot valve, 10- electromagnetical stop valve, 11- flow meter, 12- injector, 13- fuel-oil heat exchanger of control fuel, 14- engine auxiliary system, 15- engine digital electronic controller, 16- relay of fire protection system, 17-engine control lever, 18- airframe system [10.1]

11.Conclusion

Many of trade studies are made to predict as well as possible potentiality of engines. New technologies and advances calculations allows to project more efficiency mechanical devices. The engine KO-22/23 meet all of the requirements which are demanded for the next generation airliner.

To visualize the giant step of technology the KO-22/23 was compared to previous generation supersonic airliners engine Rolls-Royce Olympus. Some values are collected below

	SLS Thrust [lbf]	SLS TSFC [lb/lbf/s]	Cruise TSFC [lb/lbf/s]	Mass [lb]
KO-22/23	64650	0.487	1.036	10300
Rolls-Royce Olympus	31000	1.39	1.195	7000

Table 11.1 Comparison of previous and next generation supersonic aircraft

Used of modern technology cause increase of efficiency and reduction of manufacturing costs.

Almost no bleed short diffuser with ramp control system inlet ensure well TPR – 0.952, reduces loses and prevent unsteady work of compressor. Utilization of high pressure ratio, hollow blades, bling and blisk technologies provide effective mass reduction, approximately 50%. Moreover, transpiration cooling system used in combustor and usage of only one row of dillution holes decrease emission of NO_x and CO for about 30%. Also Turbine has its own film cooling system which increases lifetime of component, furthermore decision for using SiC/SiC CMC as main material allows to work in higher temperatures which allows to find optimal one and reduces mass. Convergent-divergent ensure high performance at all mission points. To reduce acoustic emission was used advanced shape mixer, chevrons and tiles.

Parameter	Required Value	Design Value	Margin Relative to Requirement
Hot Day Takeoff Thrust [lbf]	56570	56799	0.4%
Max Thrust at Transonic Pinch Point	14278	15193	6.4%
Max Thrust at Supersonic Cruise	14685	14829.43	0.9%
TSFC at Take off	0.652	0.6147	5.7%
TSFC at Transonic Pinch Point	0.95	0.834	12.2%
TSFC at Supersonic Cruise	1.091	1.036	5.04%
Fan Diameter	89	89	0%
Bare Engine Weight (excl. inlet)	13000	10320	20.6%
Takeoff Exhaust Jet Velocity [ft/s]	1375	1250	9%
LTO NOx [g/kN]	118.14	71.8	39.2%
Supersonic Cruise NOx [g/kN]	242.01	65.3	73%

Table 11.2 Performance requirements matrix

For last 50 years of aviation people have been expecting to fly commonly, relatively cheap and fast. Nowadays after studying needs of society and due to new technology supersonic travels are closer than ever, however, even the best aircraft would not match these goals without proper propulsion like KO-22/23.

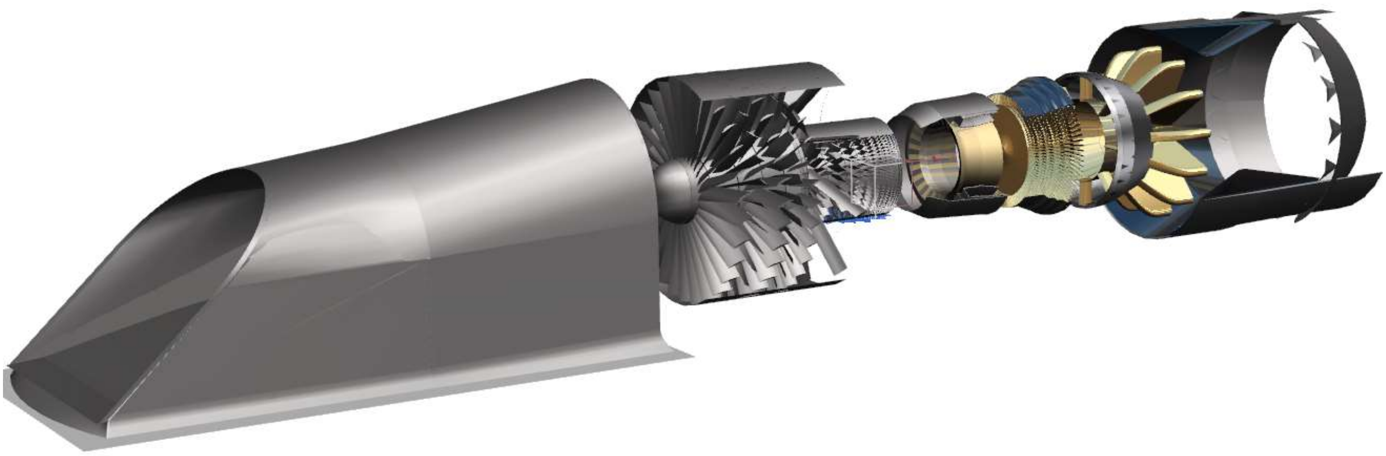

12. References

1.2 Ryszard Wiatrek, "Teoria Silników Lotniczych", Biblioteka Główna Wojskowej Akademii Technicznej, Warszawa 1983

1.1 Harry R. Welge, John Bonet, Todd Magee, Daniel Chen, Steve Hollowell, Aaron Kutzmann, Alan Mortlock, and Josh Stengle, Boeing Research & Technology, Huntington Beach, California, Chet Nelson, Eric Adamson, Steve Baughcum, Robert T. Britt, and Gregory Miller, Boeing Commercial Airplanes, Seattle, Washington, Jimmy Tai, Georgia Institute of Technology, Atlanta, Georgia, NASA/CR-2010-216842 "N+2 Supersonic Concept Development and Systems Integration"

2.1 N+2 Supersonic Concept Development and Systems Integration Harry R. Welge, John Bonet, Todd Magee, Daniel Chen, Steve Hollowell, Aaron Kutzmann, Alan Mortlock, and Josh Stengle Boeing Research & Technology, Huntington Beach, California Chet Nelson, Eric Adamson, Steve Baughcum, Robert T. Britt, and Gregory Miller Boeing Commercial Airplanes, Seattle, Washington Jimmy Tai Georgia Institute of Technology, Atlanta, GeorgiaNASA/CR-2010-216842

3.1 Saeed Farokhi, „Aircraft Propulsion Second Edition", John Wiley & Sons Ltd, 2014.

3.2 John W. Slater, "SUPIN: A Computation Tool for Supersonic Inlet Design", NASA John H. Glenn Research Center, Cleveland, Ohio 44135.

3.3 John W. Slater, "Design and Analysis Tool for External-Compression Supersonic Inlets", NASA John H. Glenn Research Center, Cleveland, Ohio 44135.

3.4 Critical Propulsion Components Volume 4: Inlet and Fan/Inlet Accoustics Team, Pratt & Whitney West Palm Beach, Florida General Electric Aircraft Engine Cincinnati, Ohio, NASA/CR—2005-213584/VOL4.

3.5 Todd E. Magee, Peter A. Wilcox, Spencer R. Fugal, and Kurt E. Acheson Boeing Research and Technology, Huntington Beach, California Eric E. Adamson, Alicia L. Bidwell, and Stephen G. Shaw Boeing Commercial Airplanes, Seattle, Washington, "System-Level Experimental Validations for Supersonic Commercial Transport Aircraft Entering Service in the 2018-2020 Time Period Phase I Final Report", NASA/CR–2013-217797.

3.6 Paul J. Barnhart, "IPAC – Inlet Performance Analysis Code", NYMA, Inc. Engineering Services Division Brook Park, OH 44142.

3.7 Stefan Szeciński, Włodzimierz balicki, Ryszard Chachurski, Paweł Głowacki, Krzysztof Kawalec, Adam Kozakiewicz, Jerzy Szczeciński, "Lotnicze zespoły Napędowe", Wojskowa Akademia Techniczna, Warszawa 2009.

3.8 United States Patent Adamson et al. "Supersonic Elliptical Ramp Inlet", US 9,447,731 B1, Sep. 20, 2016.

3.9 Ryszard Chachurski, Piotr Waślicki - Instalacje przeciwoblodzeniowe i odladzające statków powietrznych , Wojskowa Akademia Techniczna, Warszawa 2011

4.1 M. Łagosz, S. Szczeciński, „Konstrukcja silników lotniczych- wybrane zagadnienia wytrzymałości i dynamiki konstrukcji", Warszawa, 1985.

4.2 S. Szczeciński, W. Balicki, R. Chachurski, P. Głowacki, J. Godzimirski, A. Kozakiewicz, Z. Pągowski, J.Szczeciński, „Lotnicze zespoły napędowe, cz. 2", Warszawa, 2011.

4.3 S. Szczeciński, W. Balicki, R. Chachurski, P. Głowacki, J. Godzimirski, A. Kozakiewicz, Z. Pągowski, J.Szczeciński, K.Kawalec, A. Rowiński, „Lotnicze silniki turbinowe, cz.2", Warszawa, 2012.

4.4 Z. Dżygadło, „Napędy lotnicze- Zespoły wirnikowe silników turbinowych", Warszawa, 1982.

4.5 P. Dzierżanowski, „Turbinowe silniki odrzutowe", Warszawa, 1983.

4.6 M. Losertova, „Advanced material', Ostrova, 2014.

4.7 JOHN J. BRENNAN, KARL M. PREWO, "Silicon carbide fibre reinforced glass-ceramic matrix composites exhibiting high strength and toughness", United Technologies Research Center, East Hartford, CT 06109, USA.

4.8 "Jet engines", Rolls-Royce, 5th edition (fans & compressors)

4.9 Farokhi, S, "Aircraft Propulsion." 2nd Edition, John Wiley & Sons Ltd, West Sussex, United Kingdom, 2014

5.2 Michael J. Verrilli, Lisa C. Martin Glenn, Research Center, Cleveland, Ohio, David N. Brewer, U.S. Army Research Laboratory, Glenn Research Center, Cleveland, Ohio, NASA/TM—2002-211509, "RQL Sector Rig Testing of SiC/SiC Combustor Liners"

5.4 T. Yamamoto, K. Shimodaira, S. Yoshida, Y. Kurosawa, "Emission Reduction of Fuel-Staged Aircraft Engine Combustor Using an Additional Premixed Fuel Nozzle", Clean Engine Team, Aviation Program Group, Japan Aerospace Exploration Agency, 7-44-1 Jindaiji-higashi-machi, Chofu, Tokyo 182-8522, Japan

5.5 Lefebvre H. A. and Ballal R. D., "Gas Turbine Combustion", 2nd ed., CRCPress, Florida, 2010

5.6 Ryszard Łapucha, "Komory spalania silników turbinowo-odrzutowych" - procesy, obliczenia, badania, 21, Bibliotek Naukowa Instytutu Lotnictwa, Warszawa 2004

6.1 Dżygadło Z. „ Zespoły wirnikowe silników turbinowych" wydawnictwo komunikacji i łączności Warszawa 1982

6.2 Dzierżanowski P. Konstrukcja silników lotniczych. Projektowanie przejściowe i dyplomowe. Warszawa 1972

6.3 Schmid and Kalpakjian. Manufacturing Processes for Engineering Materials, 5th Ed. University of Notre Dame

6.4 -Nageswara Rao Muktinutalapati (2011). Materials for Gas Turbines – An Overview, Advances in Gas Turbine Technology, Dr. Ernesto Benini. VIT University. India

6.6 https://www.geaviation.com/press-release/military-engines/ge-successfully-tests-world's-first-rotating-ceramic-matrix-composite accessed 6.05.2018

6.7 https://ntrs.nasa.gov/archive/nasa/casi.ntrs.nasa.gov/20170005556.pdf accessed 6.05.2018

6.8 Zinkle, S.J, Snead, L.L. Thermophysical and Mechanical Properties of SiC/SiC Composites. Oak Ridge National Laboratory. 1998

6.9 /https://www.sciencedirect.com/science/article/pii/S0169433213017169 accessed 7.05.2018

6.10 Mattingly, J. D., Heiser, W.H. & Pratt, D. T. (2002). Aircraft Engine Design. 2nd Ed. AIAA

7.1 Pratt & Whitney West Palm Beach, Florida General Electric Aircraft Engines Cincinnati, Ohio, "Critical Propulsion Components Volume 3: Exhaust Nozzle", NASA/CR-2005-213584/VOL3.

7.2 Leonard E. Stitt, Exhaust Nozzles For Propolusion System With Emphasis on Supersonic Cruise Aircraft", NASA Reference Publication 1235, May 1990.

7.3 Deepak Thirumurthy∗,Energy Division, Rolls-Royce North America, Mount Vernon, OH 43050,Gregory A. Blaisdell†, Anastasios S. Lyrintzis‡ and John P. Sullivan, School of Aeronautics and Astronautics, Purdue University, West Lafayette, IN 47907, "Preliminary Design and Computational Analysis of an Ejector Nozzle with Chevrons", AIAA 2011-918

7.4 T. G. Tillman* and R. W. Patersont United Technologies Research Center, East Hartford, Connecticut 06108 and W. M. Presz Jr.*, Western New England College, Springfield, Massachusetts 01119, "Supersonic Nozzle Mixer Ejector", Vol 8, No.2, March-April 1992.

7.5 T.H.Frost, “Practical Bypass Mixing System for Fan Jet Aero Engines”, Mechanic Engineering Department, University of Newcastle-upon-Tyne.

7.6 INTERNATIONAL STANDARDS AND RECOMMENDED PRACTICES, Annex 16, Volume 1, Amendment 11,NTH EDITION OF VOLUME I - JULY 2014.

7.7 Magdy Adib – ECAA, Egypt, Fernando Catalano – University of San Paulo, Brazil, Jim Hileman – FAA, USA, Dennis Huff – NASA, USA, Takeshi Ito – JAXA, Japan, Alain Joselzon – Consultant, France ,Yuri Khaletskiy – CIAM, Russia, Ulf Michel – Consultant, Germany, Luc Mongeau – McGill University, Canada, Brian J. Tester – Southampton University, UK REPORT BY THE SECOND CAEP NOISE TECHNOLOGY INDEPENDENT EXPERT PANEL NOVEL AIRCRAFT-NOISE TECHNOLOGY REVIEW AND MEDIUM- AND LONG-TERM NOISE REDUCTION GOALS, INTERNATIONAL CIVIL AVIATION ORGANIZATION, MONTREAL 2014

7.8 N.Heeb, E. Gutmark, K.Kailasanath, “Impact of chevron spacing and asymmetric distribution on supersonic jet acoustics and flow’, University of Cincinnantia, OH 45220, US.

8.1 - http://www.univstainless.com/m50nil/ access 11.05.2018

9.1 S. Szczeciński, W. Balicki, R. Chachurski, P. Głowacki, J. Godzimirski, A. Kozakiewicz, Z. Pągowski, J.Szczeciński, „Lotnicze zespoły napędowe, cz. 2”, Warszawa, 2011.

10.1 S. Szczeciński, W. Balicki, R. Chachurski, P. Głowacki, J. Godzimirski, A. Kozakiewicz, Z. Pągowski, J.Szczeciński, „Lotnicze zespoły napędowe, cz. 2”, Warszawa, 2011.